ACS Catalysis

pubs.acs.org/acscatalysis

Perspective

Insight on Reaction Pathways of Photocatalytic CO_2 Conversion

Yiou Wang, Enqi Chen, and Junwang Tang*

Cite This: *ACS Catal.* 2022, 12, 7300−7316

Read Online

ACCESS | Metrics & More | Article Recommendations

ABSTRACT: Photocatalytic CO_2 conversion to value-added chemicals is a promising solution to mitigate the current energy and environmental issues but is a challenging process. The main obstacles include the inertness of CO_2 molecule, the sluggish multi-electron process, the unfavorable thermodynamics, and the selectivity control to preferable products. Furthermore, the lack of fundamental understanding of the reaction pathways accounts for the very moderate performance in the field. Therefore, in this Perspective, we attempt to discuss the possible reaction mechanisms toward all C_1 and C_2 value-added products, taking into account the experimental evidence and theoretical calculation on the surface adsorption, proton and electron transfer, and products desorption. Finally, the remaining challenges in the field, including mechanistic understanding, reactor design, economic consideration, and potential solutions, are critically discussed by us.

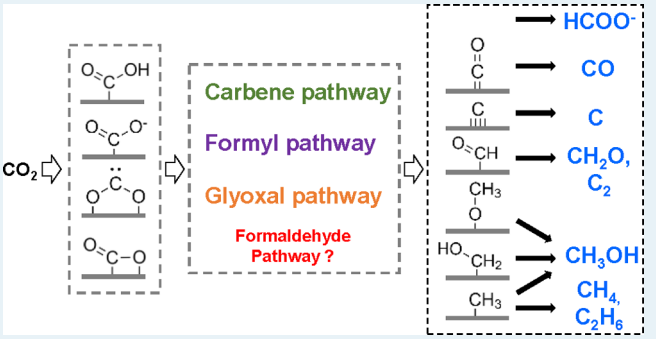

KEYWORDS: *CO_2 conversion, photocatalysis, mechanism, reaction pathways, selectivity*

1. INTRODUCTION

The atmospheric CO_2 content has inevitably increased from 275 ppm to over 400 ppm since the industrial evolution, far exceeding its natural fluctuation (180−300 ppm) over the past 800 000 years because of an emission rate of more than 2 ppm per annum.[1,2] The reactions emitting CO_2, such as the combustion of fossil fuels, could directly release heat and, in most cases, also produce water that is also a greenhouse gas in its vapor form.[3] The IR-active CO_2 molecules trap the thermal radiation from the Earth's surface and the sunlight, raising the global temperature and subsequently liberating even more CO_2 by shifting the CO_2-carbonate dissolution equilibrium in the oceans.[4] Once the natural carbon-cycle capacity is overwhelmed, an adverse process leads to dramatic climate change and other environmental issues, highlighting the urgent need for artificial approaches to maintain the carbon balance by capturing CO_2 for the carbon-neutral economy.[5]

The carbon on Earth simply moves between different reservoirs because of geological and geochemical processes as well as human activities, while the total carbon amount has remained constant (Scheme 1).[6] The new technology for CO_2 utilization should at least be carbon-neutral either via exergonic pathways or endergonic ones but driven by renewable energy sources. Inspired by the fact that the majority of carbon on the Earth's surface is stored in the form of carbonates, scientists have developed thermodynamically favorable CO_2-to-carbonate mineralization technologies.[7] Recently, the concept of converting a carbon-containing fuel into carbonates and carbon-free hydrogen was reported.[8] Meanwhile, inspired by

Scheme 1. Illustration for the Natural Carbon Cycles Including CO_2 to Organic and Inorganic Pathways

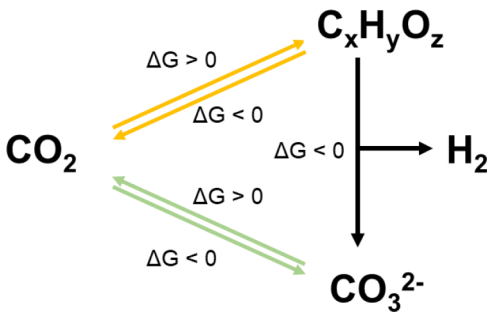

natural photosynthesis, scientists have also made significant progress in uphill reactions to fix CO_2 into high-value fuels with the input of energy from sunlight. Such sustainable solar fuels are attractive with a satisfactory density of energy stored in their chemical bonds (*e.g.*, 20 MJ/kg for methanol), which are significantly higher than current batteries (~0.1−0.7 MJ/kg) and able to be released on demand without additional carbon emission.[9−11] The storage of almost inexhaustible solar

Received: February 27, 2022
Revised: April 29, 2022
Published: June 3, 2022

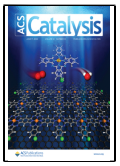

https://doi.org/10.1021/acscatal.2c01012
ACS Catal. 2022, 12, 7300−7316

energy in CO_2-reduction fuels will significantly contribute to balance the carbon-cycle and address the issues of carbon-neutral energy supply,[11] leading to the concept of the photocatalytic process for CO_2 reduction.

The earliest demonstration of photoassisted CO_2 reduction in water dates back to the late 1970s when the Pt-$SrTiO_3$ was used to convert gaseous water and CO_2 to methane, as reported by Hemminger et al., and many semiconductors (TiO_2, ZnO, CdS, GaP, and SiC) were also shown to reduce aqueous CO_2 to formic acid, formaldehyde, methanol, and methane by Inoue et al.[12,13] Since then, many efforts have been devoted not only to improve the efficiency of CO_2 photoconversion or the related but also to tune the selectivity of a specific product.[14,15] Moreover, the formation of C_{2+} products has attracted emerging attention because of their high value compared with their C_1 counterparts.[16,17] Despite the advancement made in the past decades, the performance of CO_2 photoconversion is still unsatisfactory, far from the target 10% solar-to-fuel efficiency, because of a few intrinsic reasons.

(1) The difficulty in activation of inert CO_2. Owing to the closed-shell electronic configuration, linear geometry, and $D_{\infty h}$ symmetry,[18] it requires −1.9 V potential (vs NHE at pH 7) to activate CO_2 and to form an anion radical CO_2^-, which the majority of semiconductors could hardly provide except for a few reports (*e.g.*, poly *p*-phenylene in trimethylamine).[19−22] A possible solution to lower the barrier to the reduction reaction is to adsorb CO_2 on the surface of catalysts and then reduce CO_2 together with protons, which usually requires the loading of active cocatalysts or the engineering of surficial defects such as oxygen vacancies.[19,20,23,24]

(2) The challenging multiple-electron kinetics. It is commonly believed that CO_2 reduction is a process via multi-proton and multi-electron transfer, lowering the CO_2 reduction potentials close to that of proton reduction, making it much more difficult than the two-electron proton reduction process to hydrogen.[17] Except for some reports of molecular catalysts, it is challenging to validate whether the reactions proceed via a simultaneous multi-electron transport process or through a cascade of one-electron steps, where the first electron transfer seems to be the limiting step.[25,26] Another question is whether the lifetime of the charge carriers matches that of the surface reactions of interest.

(3) Unfavorable thermodynamics of CO_2 reduction by water. Opposite to the exothermal combustion of fuels, the production of solar fuels from CO_2 and water is endothermal (*e.g.*, Gibbs free energy of 818.3 kJ/mol for CH_4 and 702.2 kJ/mol for CH_3OH).[27] Although using hydrogen instead of water could turn CO_2 reduction into exothermic reactions hence having demonstrated much-enhanced activity, these thermal catalytic processes usually proceed under higher temperatures (>150 °C) even promoted by light, requiring an additional step and energy for water electrolysis to hydrogen. Thus, hydrogenation systems and those using sacrificial hole scavengers will not be included in this Perspective as they are debatably sustainable to some extent. As the water oxidation half-reaction is very sluggish because of the four-hole chemistry and the likely oxidation of the reduction intermediates before the multi-electron carbon products are generated,[28] using water to reduce CO_2 to valuable chemicals is exceptionally challenging. In short, to overcome the obstacles mentioned above for CO_2 photoreduction, besides the commonly existing issues for photocatalysis such as light-harvesting, one has to carefully tailor the photocatalysts, cocatalysts and the reaction conditions based on the fundamental understandings.

(4) Selectivity toward preferable products. Various products could be obtained from CO_2 conversion while tuning the selectivity remains the major challenge. It should be noted that not all of the products are value-added chemicals if the cost of CO_2 capture is taken into consideration (Scheme 2).[16] For example, the commonly observed CO (with low purity) and CH_4 are economically unfavorable due to their relatively low market price. The most profitable C_1 product is formic acid, which unfortunately has a low energy content. Methanol and C_{2+} products are more attractive because of their outstanding market price, market demand, and energy content. However, because of the lack of molecular-level understanding of reaction mechanisms, the selectivity control to preferable products is still challenging.

Scheme 2. Market Price of CO_2 Recycling Products as a Function of Energy Content.[a] Reproduced from Ref 16. Copyright 2019 American Chemical Society

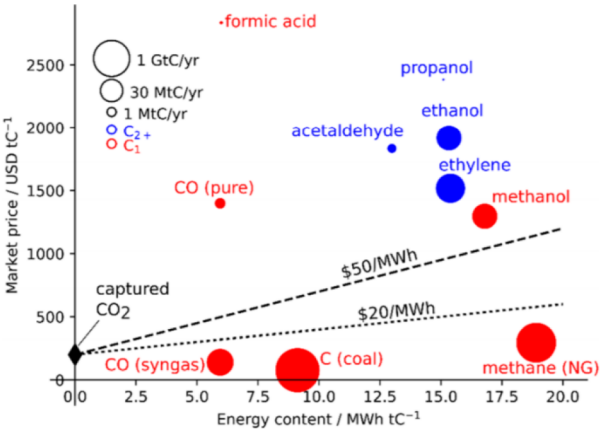

[a]Dotted lines represent minimum energy cost required for CO_2 capture and conversion based on the present commercially available technology.

Apart from the four key factors as mentioned above, the core of CO_2 photoreduction lies in the selection of semiconductor photocatalysts. The progress of semiconductor photocatalyst development has been heavily summarized by many comprehensive reviews.[20,27,29−31] Also, the strategies to design novel photocatalysts for CO_2 reduction resemble those for water splitting, which could be found in broad literatures (Scheme 3).[32−34] For example, Li et al. summarized the selectivity for photocatalytic reduction of CO_2 over different cocatalysts.[31] Briefly, Pd, Pt, or Au are more favorable for CH_4 production; Ag for CO, CH_4, or CH_3OH; Cu for hydrocarbons; and Cu_2O, RuO_2, or NiO_x for CH_3OH production. Therefore, complementary to these reviews on photocatalysts' development, here we aim to discuss the possible reaction pathways and mechanisms on the basis of our understandings in this Perspective, including how to design photocatalysts and

https://doi.org/10.1021/acscatal.2c01012
ACS Catal. 2022, 12, 7300−7316

Scheme 3. Elements Used to Construct Photocatalysts for Photocatalytic Water Splitting and Their Roles.[a] Reproduced from Ref 32. Copyright 2019 American Chemical Society

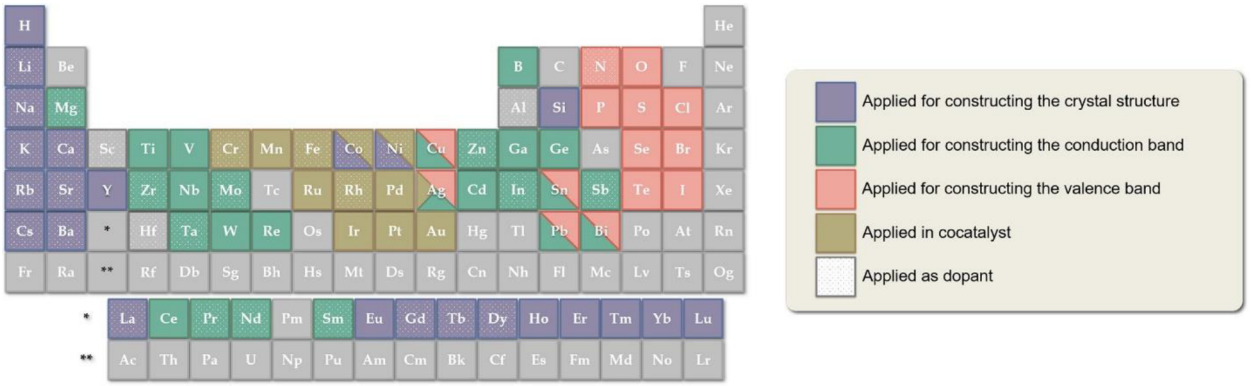

[a]Alkali metals, alkaline earth metals, and some rare-earth ions usually do not directly contribute to the formation of bands and just construct crystals structure (*e.g.*, as the A position of cations in perovskite). Most metal oxide photocatalysts are composed of metal cations with d^0 (Ti^{4+}, Zr^{4+}, Nb^{5+}, TA^{5+}, V^{5+}, W^{6+}, and Ce^{4+}) or d^{10} (Zn^{2+}, In^{3+}, Ga^{3+}, Ge^{4+}, Sn^{4+}, and Sb^{5+}) configurations. The conduction bands for d^0 and d^{10} metal oxide photocatalysts typically consist of the d and sp orbitals of the metal cations, respectively. The valence band of semiconductors usually consists of the p orbitals of N, P, O, S, Se, Te, Cl, and so on. Cocatalysts elements include, for example, Cr, Mn, Fe, Ru, Rh, Pd, Ag, Ir, Pt, Au. Some elements have more than a single function.

how to obtain this fundamental information by spectroscopies, as well as the principles for various products. Furthermore, we propose challenges facing this field, such as the characterizations needed to validate and understand the experimental process and pathways to practical applications.

2. REACTION PATHWAYS AND POSSIBLE PRODUCTS

Scheme 4 lists the redox potential of various products from photocatalytic CO_2 conversion and the band alignment of a few representative photocatalysts.[17] To determine the selectivity and efficiency of the process, gas chromatography coupled with mass spectrometry (GCMS) is commonly used to quantify the products, while for nonvolatile ionic formate or oxalate products, ion-exchange chromatography is necessary. Understanding the exact reaction mechanism of CO_2 photoreduction relies on evidence from experimental and theoretical methods. Infrared spectroscopy (IR) is helpful for surface chemistry studies, and electron paramagnetic resonance (EPR) is an essential tool to reveal the mechanism via the detection of paramagnetic unpaired electrons of the intermediates. The charge carrier dynamics could be analyzed by transient absorption measurements, together with modeling. Important information regarding adsorption and kinetics could also be provided by electrochemical measurements and theoretical computation.

Scheme 4. Band Alignments of a Few Representative Semiconductor Photocatalysts and the Related Redox Potentials to CO_2 Reduction Reactions to Different Products. Reproduced with Permission from Ref 17. Copyright 2020 American Chemical Society

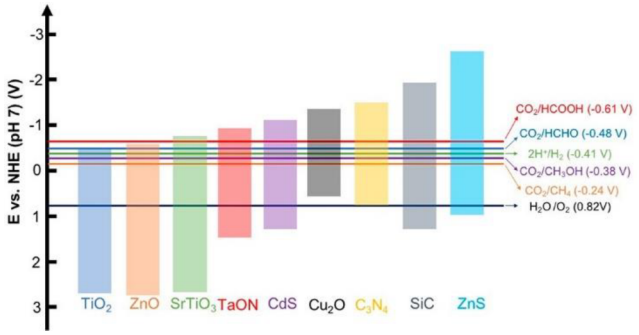

In an earlier review, Habisreutinger et al. had summarized three possible mechanisms for the photocatalytic formation of five C_1 (CO, HCOOH, CH_2O, CH_3OH, CH_4) and some C_2 products from CO_2 on TiO_2, namely the formaldehyde pathway, the carbene pathway, and the glyoxal pathway.[14] These different possibilities start with the binding modes of CO_2 on the surface of catalysts, including oxygen coordination, carbon coordination, and side/mixed coordination.[35] On the basis of these, we proposed a comprehensive description of pathways (Scheme 5). The pathways are directed by whether the following reaction occurs via electron transfer, proton transfer (sometimes hydroxyl transfer) or concerted electron–proton transfer.[16] An intermediate molecule in one pathway could be the final product of another pathway if it fast desorbs from the surface of the catalysts before further steps take place. Since the final products from the experiments are the most direct clues, we thus discuss the possible mechanistic details guided by respective products and the issues open to be elucidated.

As mentioned above, using water to reduce CO_2 is the ideal and sustainable process, which includes two half-reactions, water oxidation (eq 1) and multi-electron reduction of CO_2. The following details all these reduction processes, involving the production of C_1 (*e.g.*, formic acid, carbon monoxide, formaldehyde, carbon, methanol, and methane) and C_2 products (*e.g.*, oxalic acid, acetic acid, acetaldehyde, ethanol, ethylene, ethane) by photocatalysis.

$$\text{Oxidation reaction: } H_2O + 2h^+ \rightarrow 1/2O_2 + 2H^+,\ E_0 = 0.41\text{V vs NHE at pH} = 7 \quad (1)$$

Pathways to C_1 Products. *Two-Electron Reduction Process.* The two-electron reduction process produces CO and HCOOH on the basis of eqs 2–5, and HCOOH production happens together with water oxidation (eq 1).

https://doi.org/10.1021/acscatal.2c01012
ACS Catal. 2022, 12, 7300–7316

Scheme 5. Mechanistic Pathways of CO_2 Reduction to Commonly Observed C_1 and C_2 Products

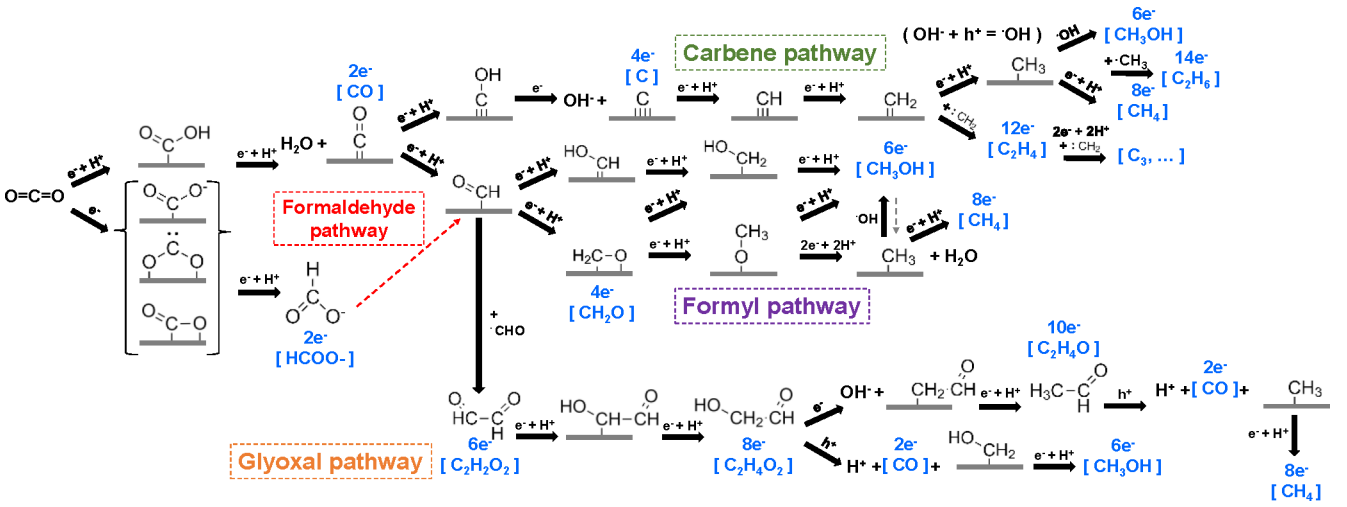

$$\text{reduction reaction: } CO_2 + 2H^+ + 2e^- \rightarrow CO + H_2O,\ E_0 = -0.53\ \text{V vs NHE at pH} = 7 \quad (2)$$

$$\text{overall reaction: } CO_2 \rightarrow CO + 1/2O_2,\ \Delta H = 283\text{kJ/mol},\ \Delta G = 257.1\text{kJ/mol} \quad (3)$$

$$\text{reduction reaction: } CO_2 + 2H^+ + 2e^- \rightarrow HCOOH,\ E_0 = -0.61\ \text{V vs NHE at pH} = 7 \quad (4)$$

$$\text{overall reaction: } CO_2 + H_2O \rightarrow HCOOH + 1/2O_2,\ \Delta H = 254.3\text{kJ/mol},\ \Delta G = 353.56\text{kJ/mol} \quad (5)$$

Carbon monoxide plays a crucial role in the Fischer−Tropsch synthesis and carbonylation of alkenes, while formic acid is a necessary preservative and antibacterial agent in livestock feed.[17] Regarding the numbers of electrons needed, CO and HCOOH are kinetically the most accessible products from CO_2, while thermodynamically, both are uphill reactions. Meanwhile, it should be noted that the minimal potential for CO_2 reduction decreases with the increase of the number of electrons involved in the products. For example, photocatalytic CO_2 conversion to CO or HCOOH requires slightly more negative potential than that to CH_4.

CO, as shown in Scheme 5, is a product, a byproduct or an intermediate in CO_2 reduction. In detail, CO is an intermediate in the carbene pathway after anchoring the C atom of CO_2 to the surface of the catalysts. One proton attacks the O atom in CO_2 to form COOH radicals in the presence of the first electron, followed by an immediate cleavage of the C−OH bond, which releases CO and water if not proceeding further.[36,37] The selectivity of this process could be controlled by the binding strength of CO on the surface of a catalyst. CO can be a poison if it binds too strongly to the metal, while CO desorbs as a final product before further reduction occurs if the binding is too weak.[38] Studies have shown that the suitable binding energy of CO on the copper catalyst and the high coverage ensures the formation of more reduced products and inhibits the competitive hydrogen evolution.[39] In the glyoxal pathway, CO is a byproduct when the C_2 intermediates decarbonylize to form methanol or methane,[40] which agrees well with the literature that CO is commonly detected together with methanol and methane products. The oxidation of organic products such as formaldehyde and methanol by photoholes also results in CO, which we observed.[41] Such backward reactions convert the kinetically more challenging reduction products to a two-electron product CO, which can be mitigated by hindering the adsorption of the formaldehyde and methanol on the oxidation sites.[41,42]

It should be noted that the selective conversion of captured CO_2 toward formic acid has been identified as one of the relatively profitable processes, although the market demand and the energy content are low (Scheme 2). Formate might be the most accessible product as all three binding modes can possibly lead to formate production (Scheme 5). Moreover, it only requires two electrons and one proton to form formate, and the breaking of the C−O bond does not occur during the formation of HCOOH. So far, the benchmark efficiency in photocatalytic CO_2 reduction was achieved in a formate production system reaching a solar-to-formate conversion efficiency of 0.08 ± 0.01% on a Z-scheme system of $SrTiO_3$:La,Rh/Au/$BiVO_4$:Mo modified with molecular cocatalysts (Scheme 6).[43]

HCOOH has been previously proposed as an intermediate in the formaldehyde pathway via the surface adsorption involving O, including bidentate and monodentate O coordination or the mixed C−O coordination.[44] EPR studies by Shkrob et al. demonstrated that only when CO_2^- radical is

Scheme 6. (a) An Energy Diagram Depicting the Photosynthetic CO_2RR Coupled with Water Oxidation. The Reduction Potentials Are Given versus the NHE at pH 6.7. Reproduced with Permission from Ref 43. Copyright 2020 Springer Nature Publishing AG

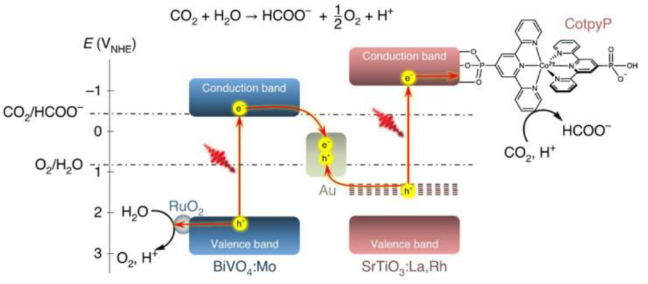

https://doi.org/10.1021/acscatal.2c01012
ACS Catal. 2022, 12, 7300−7316

doubly bound through its oxygens to the metal ions at the surface can this radical be further reduced to formate. Otherwise, the reduction is stalled.[45] The bidentate binding of the CO_2 via both O atoms results in the proton attaching to the C atom in CO_2^- to form the formate HCOO radical, which further accepts one electron and proton to form HCOOH, being a favored reaction in water with a high dielectric constant.[46,47] Regarding the further reduction of formic acid, Koci et al. showed the profiles of produced CH_4 and CH_3OH disagreed with the formaldehyde pathway, as CH_3OH is not observed as an intermediate of CH_4.[48] Hori et al. also suggested that formate is more likely the terminal product for electrochemical CO_2 reduction on copper except for systems with very high concentrations, high cathodic bias, and highly acidic or basic electrolytes.[49] Therefore, we did not wholly draw the proposed debatable formaldehyde pathway (gray dashed lines) in Scheme 5. Instead, we summarize a new formyl pathway from the literature discussed in detail below.

Four-Electron Reduction Process. The four-electron reduction process produces HCHO and C on the basis of eqs 6−9, while HCHO production requires water oxidation (eq 1).

$$\text{reduction reaction: } CO_2 + 4H^+ + 4e^- \rightarrow HCHO + H_2O,\ E_0 = -0.47\ \text{V vs NHE at pH} = 7 \quad (6)$$

$$\text{overall reaction: } CO_2 + H_2O \rightarrow HCHO + O_2,\ \Delta H = 570.73\text{kJ/mol},\ \Delta G = 541.96\text{kJ/mol} \quad (7)$$

$$\text{reduction reaction: } CO_2 + 4H^+ + 4e^- \rightarrow C(s) + 2H_2O,\ E_0 = -0.2\ \text{V vs NHE at pH} = 7 \quad (8)$$

$$\text{overall reaction: } CO_2 \rightarrow C + O_2,\ \Delta H = 393.5\text{kJ/mol},\ \Delta G = 394.38\text{kJ/mol} \quad (9)$$

Formaldehyde is helpful for disinfection and is a precursor to more complex compounds in industry. In the proposed formyl pathway (Scheme 5), if the catalyst has moderate adsorption strength, the C-anchored CO intermediate can accept one electron while a proton attacks the C atom, forming the formyl intermediate (CHO), as shown in Scheme 5, which could further be converted to CH_2O with the other proton−electron pair.[38] By calculation of Gibbs free energy differences and the energy barriers, Cheng et al. showed that adding the proton to C (forming CHO) is preferable to adding to O (forming COH) on Cu (100), which leads to the reaction toward the formyl pathway over the carbene pathway.[50] Formaldehyde could then be formed after receiving another pair of electron and proton. If the formaldehyde is not desorbed, the path further leads to CH_x species that can produce methane, as observed experimentally.[44] Cheng et al. also calculated that although CH_2O has been detected as a product, the energy barrier of CH_2O formation is 0.47 eV higher than for CHOH and hence is kinetically unfavorable.[50] In other words, reactions on Cu (100) should more likely have CHOH as an intermediate. CH_2O is detectable as a product only if it is not strongly chemically bonded to the oxide surface. Nie et al. suggested that the COH intermediate more likely exists on Cu (111), since the CHO intermediate needs to overcome a significant energy barrier, blocking further reactions to produce CH_3OH and CH_4 by calculation study.[51] Therefore, it is concluded that the exposed surface facets dominate the products and pathways.

However, Park et al. proposed an oxygen vacancy mediated mechanism to release formaldehyde on an rGO-grafted NiO-CeO_2 sample (Scheme 7).[52] The CeO_2 surface and $CO_2^{\bullet-}$

Scheme 7. Photocatalytic CO_2 Reduction Process on NiO/CeO_2/rGO Hybrid Composite Photocatalyst[a] Reproduced with Permission from Ref 52. Copyright 2021 Elsevier

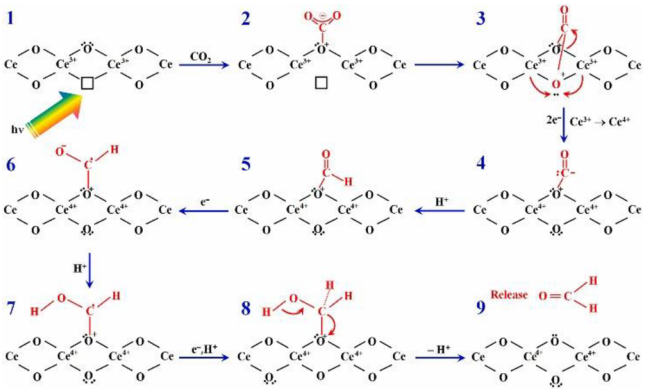

[a]Reaction mechanism and pathways associated to photoactivation of CO_2 molecules at oxygen vacancy sites of CeO_2 surface and CO_2 reduction through proton-coupled electron transfer processes at different stages of reaction.

radicals were monitored by *in situ* X-ray absorption near edge structure (XANES), *in situ* attenuated total reflectance infrared (ATR-IR) and *in situ* EPR, and then a detailed description of the multistep CO_2 photoreduction process was illustrated. Briefly, CO_2 capture occurs at the oxygen site adjacent to oxygen vacancy. One O atom from the CO_2 molecule fills the vacancy site, and the C−O bond is broken. The formation of CHO, CHOH, and CH_2OH occurs through a few electron and proton transfer processes, and then formaldehyde is produced. The formation of oxygen vacancies is due to solar light illumination, which could be validated by *in situ* XANES spectroscopy. Hence the catalytic process is sustainable, and this also indicates that a combination of these characterization techniques can reveal the mechanism in a straightforward way.

Carbon could also be formed as a four-electron product in the carbene pathway. When the proton attacks the O atom of the adsorbed CO followed by eliminating one OH^- (or with another proton to eliminate one H_2O), carbon radicals are generated (Scheme 5).[14] Such a process has been verified by the signals of the C residue on the surface detected by EPR spectroscopy.[36] DeWulf et al. also observed graphitic carbon species by X-ray photoelectron spectroscopy (XPS) and Auger electron spectroscopy (AES).[53] Such surface carbon product or intermediate could further be reduced to CH, CH_2, and CH_3 over relatively low barriers.

Besides, three theoretical models have been proposed to investigate the CO_2 reduction process via the formyl pathway, including implicit solvent models, explicit solvent models, and the H-shutting model.[16] In the implicit solvent model, a continuous description of the ions is included, whereas the explicit solvent model offers an atomistic-level picture of solvation and cation effects.[54] Furthermore, the H-shuttling model considers that water molecules shuttle the protons, and CHO radicals are formed via a direct transfer of H.[55] However,

https://doi.org/10.1021/acscatal.2c01012
ACS Catal. 2022, 12, 7300−7316

on the Cu surface, explicit calculations concluded that all steps after the formation of CO radicals are proton−electron transfers. The inconsistencies in the explanation for CO_2 reduction pathways come from both different study methods and the intrinsic complexity of the reaction mechanism. Clearly, more efforts are required to clarify this ambiguous pathway, and the combination of state-of-the-art operando spectroscopies can provide a strong potential to acquire the solution to this.

Six-Electron Reduction Process. The six-electron reduction process produces CH_3OH on the basis of eqs 10 and 11, together with water oxidation (eq 1).

$$\text{reduction reaction: } CO_2 + 6H^+ + 6e^- \rightarrow CH_3OH + H_2O,\ E_0 = -0.38\ \text{V vs NHE at pH} = 7 \quad (10)$$

$$\text{overall reaction: } CO_2 + 2H_2O \rightarrow CH_3OH + 3/2O_2,\ \Delta H = 726.13\ \text{kJ/mol},\ \Delta G = 701.93\ \text{kJ/mol} \quad (11)$$

In the suggested "methanol economy" by Olah et al., methanol could be a crucial alternative to fossil fuels as it is a suitable energy-storage material, a fuel, and a feedstock to synthesize hydrocarbons and their products.[56] In the context of the "hydrogen economy", methanol is also regarded as a promising liquid medium to store hydrogen safely and efficiently before use.[57] Methanol contains 40% more hydrogen mass density (kg H_2 per m^3) as well as over 80% more volumetric energy density than liquid H_2. In contrast, the energy for compression and liquefaction of H_2 accounts for 10−15% and 30−40% of the energy contained, respectively.[58−60] Methanol also has a suitable balance between market demand, market price, and energy content (Scheme 2). Therefore, photocatalytic CO_2 conversion by water to methanol with a high selectivity has attracted substantial attention. The reduction potential (−0.38 V vs NHE at pH = 7) is slightly more positive than proton reduction (−0.41 V vs NHE at pH = 7); hence, a large group of photocatalysts reported for hydrogen production could be applied. However, the 6-electron process of methanol generation requires an exceptionally prolonged lifetime of charge carriers for accumulation. Moreover, the oxidation of methanol with holes (∼10 ns) on TiO_2 is kinetically much more favored over water oxidation (up to ∼1 s), making the continuous production of methanol with high select ivity a significant challenge.[41]

In the carbene pathway, the C radicals continue to accept three electron−proton pairs, forming the methyl CH_3 radicals. Methanol could then be produced if the methyl CH_3 radical recombines with a hydroxyl radical ($^{\bullet}OH$).[14] In this case, methanol is not intermediate to CH_4, and formaldehyde was not formed at all. Electrochemical studies also support that methanol could not be reduced to form methane.[53,55] Instead, CH_3OH is a competitive product to CH_4, depending on a few factors such as the hydrophilicity of the surface and water amount.[61,62] The kinetic model of such a mechanism agrees with the experiment results of methanol and methane production reported by Tan et al. and Koci et al. based on TiO_2.[37,48] CO is commonly observed in experiments with methanol as the major product since CO is an intermediate in this mechanism.

In another C-coordinated formyl pathway, the adsorbed CO was not dehydrated to C radicals but was attacked by electron−proton pairs. Interestingly, despite the variety of proposed paths how the electron and protons are bought to the CO radical intermediate, namely, CHO/COH or CHOH/CH_2O, it seems that they eventually all lead to CH_2OH and CH_3O, as shown in Scheme 5, which possibly desorb as a CH_3OH, although not all the intermediates are evidenced by experiments.[16,29] Lum et al. carried out an electroreduction experiment of $C^{16}O_2$ in $H_2{}^{18}O$ on various Cu surfaces to identify the mechanism and found that CH_3OH was not ^{18}O rich, and it was only detected on Cu (111).[63] This interesting experiment shows the face-dependent selectivity of CO_2 reduction and, more importantly, indicates that the O in CH_3OH comes from CO_2 at the beginning instead of water. This result suggests that the formyl pathway or glyoxal pathway is more likely for methanol production than the carbene pathway, where OH radicals might come from water. Cheng et al. reported that at low pH, the intermediate CHOH underwent the dehydrating process, which led to the formation of CH_3 radicals and then a higher selectivity to CH_4 over CH_3OH. In contrast, a high pH, more hydrophobic environment, weak hydrogen bonding solvent, or gaseous phase benefits the selectivity toward CH_3OH.[50] In fact, methanol is very often a competitive product to CH_4 in all the proposed pathways in Scheme 5, including the glyoxal pathway. It should be noted that the production of methanol is very challenging, as the final step of releasing methanol in both the carbene pathway and formyl pathway require hydroxyl radicals, and the glyoxal pathway involves photoholes, both of which are highly oxidative. The upper routine to methanol in the formyl pathway (Scheme 5), where the intermediates are continuously bonded via carbon to avoid the oxidation of intermediates, prefers to produce methanol with high selectivity.

The stable production of methanol not only relies on the sufficient transport of electron−proton pairs but also depends on whether the produced methanol could be protected from the strongly oxidative nature of photoholes. The backward reaction of methanol oxidation could be determined by the CO yield in the products. A strategy to avoid such an issue is to suppress the adsorption of the methanol on these oxidation sites and to promote the kinetically sluggish oxidation of water against methanol. One can know whether the holes oxidize water or methanol by measuring stoichiometry between reduction and oxidation products during CO_2 reduction. We have recently reported a unique hole-accepting carbon-dots cocatalyst (CD), where water instead of methanol selectively adsorbs (Scheme 8).[41] Such CD prolongs the lifetime of charge carriers on pristine and oxygen-doped carbon nitride photocatalysts by 6−8 folds, resulting in the almost unity selectivity to methanol with stoichiometric oxygen production and internal quantum yields (IQYs) of 2−6% at 420 nm.[42,64] A transient absorption spectroscopic investigation shows that extraction of holes by the CD is critical for the remarkable performance. Under visible light, methanol can be readily oxidized to CO by photoholes of carbon nitride (CN), while on the CD-decorated CN, no CO was detected, consistent with that methanol could not be readily adsorbed on the surface of CD where holes accumulate, and photooxidation of water occurs.

Eight-Electron Reduction Process. The eight-electron reduction process produces CH_4 on the basis of eqs 12 and 13, together with water oxidation (eq 1).

https://doi.org/10.1021/acscatal.2c01012
ACS Catal. 2022, 12, 7300−7316

Scheme 8. (a) Charge Carrier Populations of Electrons and Holes Determined from Spectral Deconvolution of the TAS Spectra for FAT, CD/FAT, CN, and CD/CN samples. (b) Schematic Diagram of Photocatalytic CO_2 Reduction by the CD/FAT. (c) Methanol Oxidation Tests in the Presence of Light and CN, ^{m}CD/CN Catalysts. Reproduced with Permission from Refs 41, 42. Copyright 2020 Springer Nature Publishing AG. Copyright 2021 Wiley-VCH

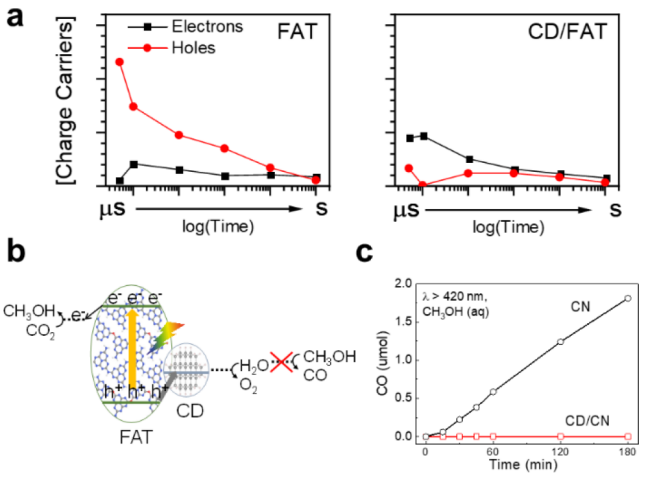

$$\text{reduction reaction: } CO_2 + 8H^+ + 8e^- \rightarrow CH_4 + 2H_2O,\ E_0 = -0.24\ \text{V vs NHE at pH} = 7 \quad (12)$$

$$\text{overall reaction: } CO_2 + 2H_2O \rightarrow CH_4 + 2O_2,\ \Delta H = 890.31\ \text{kJ/mol},\ \Delta G = 817.9\ \text{kJ/mol} \quad (13)$$

Methane is not only fuel but also a precursor for syngas, hydrogen, and methanol via its reforming.[65] The methane production requires the least negative reduction potential but the most significant amount of electrons in C_1 products. As discussed above, the carbene pathway for methane formation is more plausible than the formaldehyde pathway (Scheme 5) via the acceptance of four electron−proton pairs on the C radicals (Scheme 5).[14] In such a case, CO is an intermediate, and methanol is a competitive product. A low pH in an aqueous solution promotes the selectivity toward CH_4, which could also be beneficial via the modification of surface hydrophilicity by deposition of, for example, Pt NPs.[50] In the formyl pathway toward CH_3OH, the CH_3O intermediate is found using the explicit water model not to form CH_4 because of the significant barrier for proton−electron transfer from CH_3O to CH_4 + O.[35] The protonation of *CO to *CHO is the rate-determining step, which is followed by a series of proton−electron transfers to form *CHOH, *CH, *CH_2, *CH_3, and finally CH_4.[35]

Surface oxygen vacancies are commonly used strategies to modify a photocatalyst. Ji et al. proposed a mechanism for the perfect and defective surfaces by theoretical calculation (Scheme 9). They found that a fast-hydrogenation path can occur at both the surface Ti atoms and the oxygen vacancies, while the oxygen vacancies are more active than the surface Ti atoms for the reaction. The fast-hydrogenation path at the oxygen vacancies combines the hydrogenation and deoxygenation paths.[66] This pathway agrees with the experimental results because CH_3OH and CH_4 often appear simultaneously

Scheme 9. Mechanism for the Photoreduction of CO_2 on the Perfect (Black) and Defective (Red) Surfaces. Reproduced from ref 66. Copyright 2016 American Chemical Society

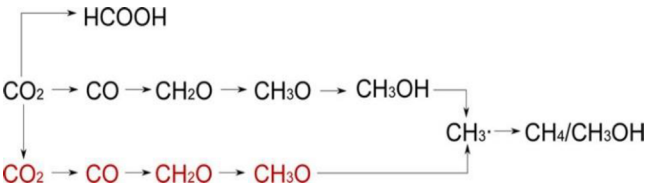

and explain the possible formation of formic acid and formaldehyde.

As discussed above, the existence of more active intermediates, including formaldehyde and methanol in the presence of highly oxidative photoholes, contradicts the formaldehyde pathway for CH_4 formation, in that one-electron reduction of these molecules in the reaction is energetically prohibitive.[38] Shkrob et al. found that reaction barriers for further reduction could be significantly lowered by joining two carbon atoms and proposed to follow the glyoxal $(CHO)_2$ pathway toward CH_4 involving a number of C_2 compounds (Scheme 10). In this pathway, the critical intermediate is the glyoxal (or ethanediol), produced from the dimerization of formyl radicals CHO radicals (Scheme 5).[40] Because of its π-conjugation, glyoxal is still a much more efficient electron acceptor than formaldehyde, which can be step-by-step reduced to glycolaldehyde (HOCHCHO), acetaldehyde (CH_2CHO), and acetaldehyde. These C_2 molecules can be further oxidized to an unstable acetyl radical, which undergoes decarboxylation to a methyl radical. The recombination of the methyl radical with a hydrogen atom forms CH_4. Formate, methanol, and formaldehyde are intermediates all formed in this pathway and serve as sacrificial hole scavengers. The glyoxal pathway will be further discussed later.

The representative examples of photocatalytic systems of CO_2 reduction to C_1 products have been summarized in Table 1. Considering the economic potential of the C_1 products such as formate/formic acid and methanol, the efficient systems for these products are of particular interest. For example, the highest solar-to-fuel efficiency of 0.08 ± 0.01% (solar-to-formate) measured under the solar simulator was achieved on the molecular cocatalyst coated on a Z-scheme particulate sheet (phosphonated Co(II) bis(terpyridine) and RuO_2 catalysts modified $SrTiO_3$: La, Rh|Au| $BiVO_4$: Mo).[43] The benchmark system for CO_2 photoreduction to formic acid was based on a gas-permeable metal−organic framework (MOF) with an apparent quantum efficiency (AQE) of 15.76% at 420 nm, at the porous gas−solid interfaces with a near-unity selectivity.[67] Such a high quantum efficiency is also the highest among most systems for the C_1 products, suggesting that the metal−organic complexes play a significant role in CO_2 reduction. More examples of metal complex photocatalysts could be found in other reviews.[26] The highest internal quantum efficiency at 420 nm toward methanol was measured on carbon dots/oxygen-doped carbon nitride.[42] The key to maintaining a reasonable efficiency of methanol is to mitigate overoxidation of methanol product to CO.

Pathways to C_2 Products. The direct photoconversion of CO_2 to C_2 products is more attractive because of their significantly higher market price and energy content per carbon compared with the C_1 products (except for methanol in

https://doi.org/10.1021/acscatal.2c01012
ACS Catal. 2022, 12, 7300−7316

Scheme 10. "Glyoxal Cycle".[a] Reproduced from Ref 40. Copyright 2012 American Chemical Society

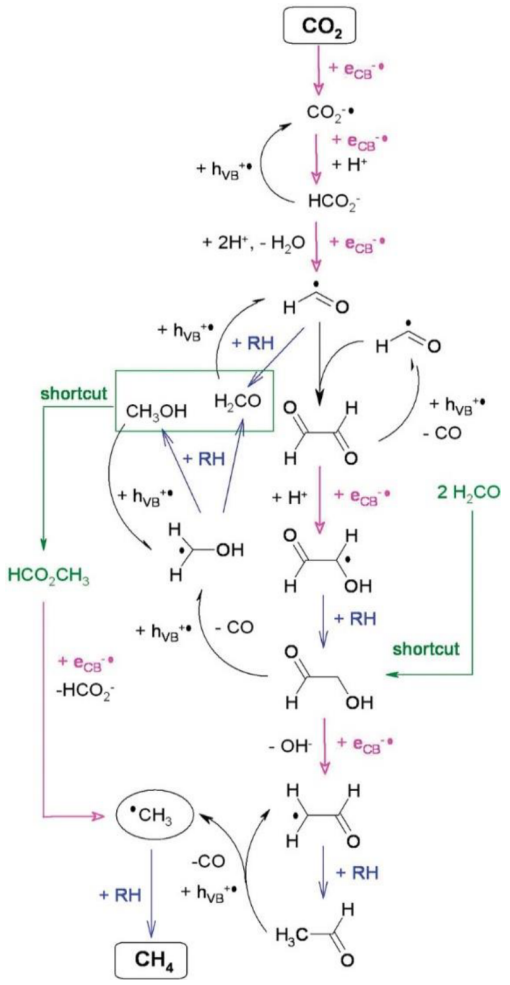

[a]In this scheme, RH stands for the generic (molecular or radical) donor of H atoms.

Scheme 2).[16] The formation of the C−C bond by dimerization of C_1 intermediates on the surface of catalysts is the key to further producing C_2 products. For example, the pathways toward ethylene or ethane involve the coupling of carbene intermediates (CH_2, CH_3) in the carbene pathway while the dimerization of formyl (CHO) in the glyoxal pathway can result in a variety of C_1 and C_2 products (Scheme 5). These pathways mostly require multiple electrons and protons, which will be favorable on the surface with an increased density of charge carriers and protons. Also, the binding of intermediates on the surface of the catalysts must be sufficiently strong to reach the C_2 products instead of desorbing them early as C_1 products such as CO and CH_2O. C_1 products such as CO, CH_4, and CH_3OH can also be byproducts of these processes. All these processes again share the water oxidation half-reaction (eq 1). The following lists the chemical eqs (eqs 14−25) for C_2 products with 2 to 14 electrons, respectively.

Two-Electron Reduction Process. The two-electron reduction process produces $(COOH)_2$ on the basis of eqs 14 and 15.

$$\text{reduction reaction: } 2CO_2 + 2e^- + 2H^+ = (COOH)_2,\ E_0 = -0.88\ \text{V vs NHE at pH} = 7 \quad (14)$$

$$\text{overall reaction: } 2CO_2 + H_2O = (COOH)_2 + \frac{1}{2}O_2,\ \Delta H = 458.6\ \text{kJ/mol},\ \Delta G = 460.42\ \text{kJ/mol} \quad (15)$$

Eight-Electron Reduction Process. The eight-electron reduction process produces CH_3COOH on the basis of eqs 16 and 17.

$$\text{reduction reaction: } 2CO_2 + 8e^- + 8H^+ = CH_3COOH + 2H_2O,\ E_0 = -0.3\ \text{V vs NHE at pH} = 7 \quad (16)$$

$$\text{overall reaction: } 2CO_2 + 2H_2O = CH_3COOH + 2O_2,\ \Delta H = 874.53\text{kJ/mol},\ \Delta G = 873.17\text{kJ/mol} \quad (17)$$

Ten-Electron Reduction Process. The 10-electron reduction process produces CH_3CHO on the basis of eqs 18 and 19.

$$\text{reduction reaction: } 2CO_2 + 10e^- + 10H^+ = CH_3CHO + 3H_2O,\ E_0 = -0.3\ \text{V vs NHE at pH} = 7 \quad (18)$$

$$\text{overall reaction: } 2CO_2 + 2H_2O = CH_3CHO + \frac{5}{2}O_2,\ \Delta H = 1166.96\ \text{kJ/mol},\ \Delta G = 1129.56\ \text{kJ/mol} \quad (19)$$

Twelve-Electron Reduction Process. The 12-electron reduction process produces CH_3CH_2OH and C_2H_4 on the basis of eqs 20−23.

$$\text{reduction reaction: } 2CO_2 + 12e^- + 12H^+ = CH_3CH_2OH + 3H_2O,\ E_0 = -0.32\ \text{V vs NHE at pH} = 7 \quad (20)$$

$$\text{overall reaction: } 2CO_2 + 3H_2O = CH_3CH_2OH + 3O_2,\ \Delta H = 1090.53\ \text{kJ/mol},\ \Delta G = 1470.31\ \text{kJ/mol} \quad (21)$$

$$\text{reduction reaction: } 2CO_2 + 12e^- + 12H^+ = C_2H_4 + 4H_2O,\ E_0 = -0.33\ \text{V vs NHE at pH} = 7 \quad (22)$$

$$\text{overall reaction: } 2CO_2 + 2H_2O = C_2H_4 + 3O_2,\ \Delta H = 1411.06\ \text{kJ/mol},\ \Delta G = 1324.52\ \text{kJ/mol} \quad (23)$$

Fourteen-Electron Reduction Process. The 14-electron reduction process produces C_2H_6 on the basis of eqs 24 and 25.

$$\text{reduction reaction: } 2CO_2 + 14e^- + 14H^+ = C_2H_6 + 4H_2O,\ E_0 = -0.27\ \text{V vs NHE at pH} = 7 \quad (24)$$

$$\text{overall reaction: } 2CO_2 + 3H_2O = C_2H_6 + 7/2O_2,\ \Delta H = 1559.81\ \text{kJ/mol},\ \Delta G = 1467.5\ \text{kJ/mol} \quad (25)$$

Since the pathways to C_2 products are believed to involve both multi-electron coupled proton transfer and the C−C coupling processes, the reactions are generally more challenging, and fewer reports have achieved high selectivities.[80] Different from the reactions toward C_1 products, which are mostly proton-coupled one-carbon two-electron processes, the

https://doi.org/10.1021/acscatal.2c01012
ACS Catal. 2022, 12, 7300−7316

Table 1. Representative Examples for Selective Photocatalytic CO_2 Reduction to C_1 Products

final product	electron transfer	catalyst	production rate	pressure and temperature	other conditions	selectivity	efficiency
CO	2	Au-MMT/TiO_2[68]	1223 μmol g^{-1} h^{-1}	atm.; 100 °C	CO_2 and H_2, UV-light	99%	\
		Ru@Co_3O_4[69]	2003 μmol g^{-1} h^{-1}	1 atm; 15 °C	30 mL, acetonitrile/TEOA/H_2O = 3:1:1 (v/v), 300 W xenon lamp with a 420 nm cutoff filter	77%	EQE = 0.069%
		Ru@g-C_3N_4[70]	181.25 μmol g^{-1} h^{-1}	\	400W Hg lamp, 20 vol % TEOA in DMA,	64%	\
		TiO_2/$CsPbBr_3$[71]	9.02 μmol g^{-1} h^{-1}	80 kPa; 10 °C	30 mL of acetonitrile, and 100 μL of water; 300 W Xe arc lamp	95%	\
HCOOH	2	photocatalyst sheet $SrTiO_3$: La, RhlAulRuO_2−$BiVO_4$: Mo[43]	1.09 ± 0.12 μmol cm^{-2} h^{-1}	atm.	CO_2 saturated 0.1 M $KHCO_3$	97 ± 3%	solar-to-formate conversion efficiency of 0.08 ± 0.01%. AQY = 2.6% (420 ± 15 nm)
		Ru@g-C_3N_4[72]	46.425 μmol g^{-1} h^{-1}	r.t.	λ> 400 nm, 20 vol % TEOA in acetonitrile	\	\
		single metal atom @ A-aUiO[67]	3.38 mmol g^{-1} h^{-1}	\	particle-in-solution mode, and gas-membrane-gas mode	near unity	AQE = 2.51% (gas−liquid−solid reaction interface); AQE of 15.76% (porous gas−solid interfaces, 420 nm)
HCHO	4	Pt and Cu @$K_2Ti_6O_{13}$ particles[73]	3.42 μmol g^{-1} h^{-1}	r.t.	300 W Xe lamp; H_2O and CO_2	\	\
		Au NPs @TiO_2 films[74]	1.36 μmol g^{-1} h^{-1}	\	254 nm UV	\	\
		NiO/CeO_2/rGO[52]	421.09 μmol g^{-1} h^{-1}	\	0.2 M $NaHCO_3$ and 0.2 M Na_2SO_3 solution	\	solar to fuel conversion efficiency 0.775%
C	4	reduced $NiFe_2O_4$[75]	\	atm.; 80 °C	catalyst was uniformly dispersed onto the quartz glass reactor	\	\
CH_3OH	6	carbon dot/C_3N_4[41]	13.9 ± 1.7 μmol g^{-1} h^{-1}	atm.; r.t.	H_2O and CO_2	99.60%	IQY: 2.1% (420 nm), 0.7% (500 nm), 0.4% (600 nm)
		carbon nitride-like polymer (FAT) decorated with carbon dots[42]	24.2 μmol g^{-1} h^{-1}	atm.	H_2O and CO_2	100.00%	IQY: 5.9% at λ=420 nm
		carbon nitride-CdS QD[76]	186.4 μmol g^{-1} h^{-1}	\	CO_2 in 40 mL of $KHCO_3$ (0.1M) and Na_2SO_3 (0.1M)	73%	AQE = 0.91% (435 nm)
CH_4	8	$BiVO_4$/WO_3[77]	105 μmol g^{-1} h^{-1}	\	30 mL of 0.1 M NaOH, purged with high purity CO_2 for 45 min	99%	0.074% solar to methane efficiency
		Ni@SiO_2-Al_2O_3[78]	4200 μmol g^{-1} h^{-1}	150 °C	H_2 (14.5 mmol, 80 v/v %) and CO_2 (3.63 mmol, 20 v/v %); 300 W Xe lamp, 1 KW/m^2	\	\
		CoDAC-3.5 with BV NSs[79]	19.5 μmol g^{-1} h^{-1}	\	H_2O and CO_2	65%	AQY = 5.23% (400 nm)

https://doi.org/10.1021/acscatal.2c01012
ACS Catal. 2022, 12, 7300−7316

pathway to C_2 products proposed by Shkrob et al., namely the glyoxal pathway (Scheme 10), is a mainly one-electron two-carbon process through a glyoxal intermediate (*e.g.*, on TiO_2) as evidenced by EPR.[40] The reason to postulate an alternative mechanism is that no evidence of one-electron reduction intermediate (*e.g.* formate, formaldehyde, or methanol) has been observed in EPR. As mentioned above, these intermediates are more likely to be oxidized than reduced. However, the glyoxal intermediate is a strong electron acceptor, which is more facile to be reduced than oxidized. Moreover, the glyoxal pathway can provide mechanisms for C_1 products such as CO, CH_4, methanol, formate and formaldehyde and explain the possible C_2 products observed, including acetaldehyde and methylformate.

As shown in Schemes 5 and 10, different from the de−OH^- step after receiving one proton in the carbene pathway, the crucial step in the glyoxal pathway is the dehydration step after getting three protons (or de-OH^- step after accepting two protons[14]), forming formyl radicals (HC*O). Then the formyl radicals dimerize to yield glyoxal, which is reduced to trans-ethan-1,2,-semidione (HO-C*H-CHO), glycolaldehyde (HO-CH_2-CHO), and vinoxyl (*CH_2-CHO) radicals. The vinoxyl radical could be further converted to acetaldehyde (CH_3CHO) or decarbonylized to *CH_2OH, which is the precursor for methanol (CH_3OH). The acetaldehyde could be further oxidized to acetic acid or undergo decarbonylation to form methyl radicals (*CH_3), which leads to the formation of methane (CH_4). These decarbonylation processes release carbon monoxide (CO). In this case, CO is a byproduct commonly observed in CH_4 and CH_3OH production.

The most distinct difference between the glyoxal cycle and other pathways is that the former involves not only proton-coupled electron transfer but also oxidation steps. Such pathways are not possible in the absence of holes, for example, at the cathode in the electrocatalytic system. However, the existence of holes results in the production of CO rather than C_2 products. Therefore, if one targets value-added C_2 products, the oxidative conditions should be mitigated. Another interesting difference is that the glyoxal pathway has some recycling steps where some of the intermediates (*e.g.*, CH_3OH and CH_2O) serve as hole scavengers, hence replenishing the pool of formyl and hydroxymethyl radicals. Compared with C_1 products, glyoxal and methanol have the same required electrons with the number of 6, and the acetic acid and glycolaldehyde have the same electrons needed with the number of 8 as methane. The production of acetaldehyde and ethylene glycol need 10 electrons, while ethylene and ethanol need 12 electrons. It should be noted that the 10-electron product acetaldehyde is an intermediate for an 8-electron product CH_4 and a 2-electron product CO, which are much cheaper. It is not economically favorable to oxidize acetaldehyde to CH_4 and CO, considering the high numbers of demanded electrons and the low price of methane in the market. It is preferable to produce the C_2 products with those electrons. How CO_2 molecules bind on the surface of the catalysts usually determines the following steps for various possible products. In the pathways to C_2 products, C−C, C−O and single C bindings probably exist at the initial stages when forming glyoxal intermediates, and the coordination might rearrange to O−O binding during the reaction. However, it seems that a few binding modes and the following steps all can lead to products including glycolaldehyde, acetaldehyde, ethylene glycol, ethylene, and ethanol.[81]

Park et al. reported a CdS/(Cu-TNT: $Na_xH_{2-x}Ti_3O_7$) for photoconversion of CO_2 and water into C_1−C_3 hydrocarbons (*e.g.*, CH_4, C_2H_6, C_3H_8, C_2H_4, C_3H_6) under visible light without the detection of CO or H_2 (Scheme 11).[82] It could go

Scheme 11. Proposed Elementary Reaction Pathways of Photocatalytic CO_2 Conversion into Hydrocarbons. Reproduced from Ref 82. Copyright 2015 American Chemical Society

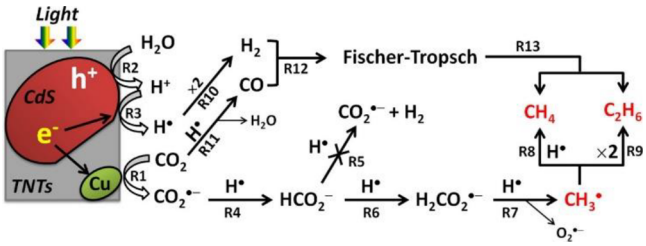

through an F−T process consuming hydrogen and CO. They also proposed that the bidentate binding of O═C═O to specific reactive surface sites reduced the energy barrier for conduction band electron transfer to CO_2. The formate radical eliminates an $O_2^{\bullet-}$ radical, forming a methyl radical. The methyl radical ($CH_3^{\bullet}$), as observed by ESR, was trapped by the copper on the surface of TNTs and then self-reacts to produce ethane.[82] This pathway indicates that the C−C coupling of methyl radicals on the surface of photocatalysts is crucial for the production of C_{2+} products such as ethane.

Regarding the C_2H_6 formation on the surface of Pt-graphene/defect-induced TiO_2, where CO_2 adsorption takes place upon abundant Ti^{3+}/V_O sites through the O atom of CO_2.[83] An alkaline surface is favorable for C_2H_6 formation by significantly improving the activation and dissociation.[84] Electrons and holes accumulate on Ti^{3+} and graphene, respectively, with Pt accelerating electron extraction. Graphene scavenges water to supply sustained protons and benefits the stabilization of $^{\bullet}CH_3$, thus promoting C_2H_6 formation, although CH_4 is also a major product.

Hori et al. and Schouten et al. showed that Cu (111) leads to lower onset overpotentials for both CH_4 formation and C_2H_4 formation, while the dimerization of CO leads to C_2H_4 as the product on Cu (100).[85,86] The dimerization of CO is followed by a few steps which are similar to the glyoxal pathway, except that the intermediate (CH_2CHO) changes from C-coordination to O-coordination. $CH_2CHO^{\bullet}$ could further produce C_2H_4 or CH_3CH_2OH.[44] It should be noted that these reports are based on studies on the electrochemical reduction of CO_2, and the pathways to C_2 products have not been observed in photocatalytic research.

There is also a possibility that C_2 products can be produced via the carbene pathway (Scheme 5). In this pathway, another carbene radical might attack the formed CH_4 or CH_3OH to make C_2H_4 or C_2H_6.[31] Other products, including C_3 and C_{3+}, could also be obtained if more carbene radicals are involved in such a mechanism but are hardly reported.[31] Kuhl et al. have proposed an enol-like intermediates pathway. However, how the enol (*e.g.*, $C_2H_4O_3$, $C_3H_6O_2$) is formed on the surface of catalysts remains unclear.[87] Strategies that increase the density of charge carriers and protons, tune the surface adsorption/desorption, and modify the surface acidity and alkalinity are believed to promote the reaction toward C_{2+} products,

https://doi.org/10.1021/acscatal.2c01012
ACS Catal. 2022, 12, 7300−7316

Table 2. Representative Examples for Selective Photocatalytic CO_2 Reduction to C_2 products

final product	electron transfer	catalyst	production rate	pressure and temperature	other conditions	selectivity	efficiency
CH_3COOH	8	partially reduced Co_3O_4 nanosheets[89]	3 μmol g^{-1} h^{-1}	25 °C	simulated air (0.03% CO_2)	92.50%	2.75% CO_2-to-CH_3COOH conversion ratio
		metal−organic framework/MoS_2[90]	39.0 μmol g^{-1} h^{-1}	0.1 MPa	H_2O and CO_2 with visible light	94.00%	\
		1%MgO@TiO_2[91]	1.04 μmol L^{-1} g^{-1} h^{-1}	25 °C	100 mL 0.1 M NaOH with CO_2 ; 253.7 nm (0.167 mW/cm2)	\	\
		WO_3·0.33H_2O[92]	9.4 μmol g^{-1} h^{-1}	4 °C	H_2O and CO_2 (50% in Ar)	85%	\
CH_3CHO	10	locally crystallized polymeric carbon nitride (PCN)[88]	1814.7 μmol g^{-1} h^{-1}	10 °C	3 mL of 10% triethanolamine (TEOA)/acetonitrile (MeCN) solution with 0.3 mL of H_2O in a 60 mL sealed flat quartz reactor	98%	quantum efficiency of 22.4% at 385 nm; QE of 13.3% at 420 nm
		bulk g-C_3N_4[93]	0.4 μmol h^{-1}	0.06 MPa	water vapor and CO_2 UV−vis light source	\	\
		C-SnS_2[94]	139 μmol g^{-1} h^{-1}	Atm.; 25 °C	300 W halogen lamp, gas flow reactor		photochemical quantum efficiency: 0.7%
		Nb-doped TiO_2[95]	572 μmol g^{-1} h^{-1}	R.t.	$NaHCO_3$ solution (0.1 M, 45 mL) with triethanolamine (5 mL) as the sacrificial agent.	98%	\
CH_3CH_2OH	12	red phosphorus decorated Bi_2MoO_6[96]	51.8 μmol g^{-1} h^{-1}	\	water vapor	\	\
		AgBr−Nitrogen doped graphene−g-C_3N_4[97]	51 μmol g^{-1} h^{-1}	r.t.	$NaHCO_3$ and CO_2, Xe lamp (450W)	\	AQY = 3.5%
		conducting polymers modified Bi_2WO_6 microspheres[98]	5.13 μmol g^{-1} h^{-1}	4 °C	H_2O and CO_2	\	AQE = 0.0086% of PTh/Bi_2WO_6
		Bi_2MoO_6 quantum dots in situ grown on reduced graphene[99]	14.37 μmol g^{-1} h^{-1}	4 °C, atm.	H_2O and CO_2	\	AQE = 0.00793% at 300 W Xe lamp with a 420 ± 15 nm band-pass filter
C_2H_4	12	C/Cu_2O mesoporous nanorods[100]	0.016 μmol h^{-1}	atm.; r.t.	0.1 M $KHCO_3$ and CO_2	56.1%	AQE= 1.36% at 400 nm
		Cu/TiO_2 powders[101]	0.542 μL g^{-1} h^{-1}	28 kgf/cm pressured CO_2	H_2O and CO_2	48.7%	\
		g-MWCNT@TiO_2 core−shell nanocomposites[102]	0.048 μmol g^{-1} h^{-1}	bubbling CO_2 in H_2O at 60 °C, Atm.	H_2O and CO_2	5%	\
C_2H_6	14	CdS/(Cu-TNTs)[82]	17 μL g^{-1} h^{-1}	20−25 °C and atm.	H_2O and CO_2, 450 W Xe lamp, 420 nm	\	\
		Nafion/Pd-TiO_2[103]	1 μmol h^{-1}	atm.; r.t.	$NaHCO_3$ aqueous dispersion CO_2 saturated, pH 1, 300 W Xe lamp (λ > 300 nm), 5 h	6.4%	\
		Pt-G/defect-induced TiO_2[83]	11 μmol g^{-1} h^{-1}	atm.; r.t.	sun simulated light (100 mW/cm^2), moist CO_2, continuous flow 1 mL min^{-1}	22.9%	AQE = 2.7%
		AuPd/(101) TiO_2[104]	1 μmol g^{-1} h^{-1}	0.26 MPa, 40 °C	$NaHCO_3$ aqueous dispersion CO_2 saturated, 300 W Xe lamp	7%	\

https://doi.org/10.1021/acscatal.2c01012
ACS Catal. 2022, 12, 7300−7316

including using a larger number of photon flux and higher energy, cocatalysts, SPR effects and surface defects.[17]

Most of the C_2 products are valuable products. As summarized in Table 2, the benchmark quantum efficiency for C_2 products is 22.4% at 385 nm and 13.3% at 420 nm (CO_2 to acetaldehyde with a 98.3% selectivity) achieved on locally crystallized carbon nitride.[88] Liu et al. used DRIFT and theoretical calculation to prove that an amino-2-propanol-assisted hydrothermal treated carbon nitride had strong bonding with the *OCCHO group, which is favorable to a C−C coupling process and changes the reaction pathway to form CH_3CHO instead of HCHO. The highest quantum efficiency for ethanol was 3.5% on AgBr−N-doped carbon nitride. While the activity and selectivity for ethylene and ethane are generally much smaller, which might result from the large numbers of electrons needed for these products (12−14 electrons).

3. CHALLENGES AND OUTLOOK

We have discussed the detailed potential pathways toward various products, including the well-established carbene pathway, glyoxal pathway and a formyl pathway. The reaction pathway and consequently the product selectivity of photocatalytic CO_2 conversion highly depends on the surface chemistry of adsorption of CO_2 and desorption of intermediates on the surface of photo/cocatalysts, which has been thoroughly summarized in other reviews (Scheme 12).[17,20,29,31,48,105] Other factors including crystal facets,

Scheme 12. Possible Adsorption of CO_2 and Desorption of Intermediates on the Surface of Cocatalysts in Photocatalytic CO_2 Reduction

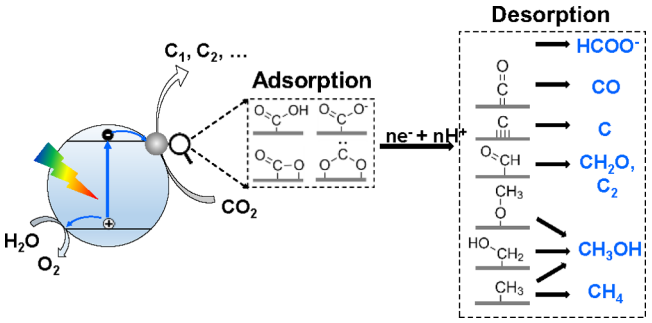

surface poisoning phenomena, which are closely related with the bonding modes and strength as discussed above, could also influence the reactivity and selectivity.[16,69,81]

The key facts of these pathways are summarized in Table 3 regarding different profiles of product distribution. For example, formate can be a promising product because it is both economically beneficial and kinetically easy to produce. However, CO exists in all the pathways. Based on the amount and production profile, the possible mechanism could be inferred. For example, if the amount of CO is minor compared with other main products, it is likely an intermediate or an oxidation product from, for example, methanol. If the amount of CO is comparable to methanol or methane, the reaction is most likely via the glyoxal pathway. Methanol and methane are always competitive products in these pathways, but methanol is more desired in the aspect of market price and transportation, providing its further oxidation could be mitigated. However, this is challenging because the final step of releasing methanol in a few pathways involves photoholes or hydroxyl radicals, which are highly oxidative. Methane requires multi-electrons (8 e^-), but its price is even below the cost of capturing CO_2. If the reaction goes through the glyoxal pathway, terminating the products at C_2 before the decarbonlization is more meaningful, rather than the decomposition of the C_2 to unprofitable CO and CH_4. Another pathway to C_{2+} products via carbene coupling is promising as it has the potential to produce long-chain products.

Although substantial progress has been made in developing and understanding photocatalysts for solar fuel production from CO_2 and water, we believe there are at least four significant challenges to overcome in this field apart from the discovery of catalysts/cocatalysts, which have been extensively reviewed by others.[16,17,27,29,31,105,106]

Validation of the Reactions. The first challenge is the confirmation of the products in CO_2 reduction reactions. In two studies, Yang et al. and Yui et al. observed ^{12}C products (^{12}CO and $^{12}CH_4$, respectively) even if $^{13}CO_2$ was used as the carbon source, indicating the carbon residues in the system could participate in the photoreactions hence should not be ignored. Therefore, the detection of all carbon-based products is not indeed proof of CO_2 reduction before the validation by control experiments. Control experiments in the CO_2 atmosphere and inert gas (*e.g.*, Argon) might give some hints. While the direct evidence is the isotopic labeling experiments, which could be carried out in a GCMS,[41] an IR system[107] or NMR[43] to distinguish the ^{13}C labeled products. Hence it is crucial for all CO_2 reduction reactions.

Meanwhile, the oxidation products (*e.g.* oxygen) should also be scrutinized and calculated with the detected carbon products to verify whether the stoichiometry of proposed reactions is achieved. Besides, the performance reported by different groups critically depends on many specific details of the experimental setup and reaction conditions, such as the light source, the pH, cocatalyst selection and loading, the sample concentration, and the reactor design. To minimize such influences, the quantum yield (QY) together with the product generation rate is all required.

Mechanism to Generate High-Value-Added Products. The second challenge is to understand the production mechanism of high-value chemicals, especially C_{2+}, via multi-electron processes since interfacial reactions such as CO_2 and multiproton reduction usually occur on a time scale of microseconds or longer.[28] As observed for CN_xH_y, such trapping leads to a severe loss of driving force and microsecond charge transfer rate.[108] To obtain a sufficient charge carrier lifetime without losing too much driving force for the interface redox reaction, nature uses a dual photocatalyst system instead of a single photocatalyst, allowing the realization of effective charge separation via a series of downhill charge transfers and overcome the inevitable back reaction.[109] There were reports on the Z-scheme CO_2 reduction systems, in which electrons and holes are generated on the spatially separated subsystems, thereby reducing the tendency of electron−hole recombination and allowing a longer lifetime and more significant accumulation of charge carriers to overcome the kinetic limitations.[43] The accurate determination of the time scale of the charge carrier relaxation and the excited state as well as the respective reaction intermediates at the surface will provide us with the information needed to design effective materials for the selective production of the high-value products. This

https://doi.org/10.1021/acscatal.2c01012
ACS Catal. 2022, 12, 7300−7316

Table 3. Summary of Important Facts for the Diverse Products from Photocatalytic CO_2 Conversion by Three Proposed Pathways

products	remarks	carbene pathway	formyl pathway	glyoxal pathway
$HCOO^-$	high market price, one-step final product, no C−O breaking, accessible from various binding modes	×	×	×
CO	uneconomic if produced with H_2, while valuable if pure CO, may exist in all pathways	intermediate and final product if weak binding	intermediate, byproduct from *e.g.* methanol oxidation	intermediate, final byproduct to methanol or methane
C	uneconomic	intermediate and product	×	×
CH_2O		×	intermediate and product	intermediate and product
CH_3OH	high energy content, valuable liquid fuel	the final competitive product to methane	the final competitive product to methane	the final competitive product to methane, release with CO
CH_4	high energy content but Uneconomic	the final competitive product to methanol	the final competitive product to methanol	the final competitive product to methanol, release with CO
C_2H_4, C_2H_6	high energy content and high market price	product from carbene coupling	×	×
$C_2H_2O_2$, $C_2H_4O_2$, C_2H_4O	high energy content and high market price	×	×	intermediate and final product if not further decarbonlised

information can be obtained by *in situ* spectroscopies such as IR, EPR, XPE, XANES, and theoretical calculation.

Practical Devices. The third challenge is to develop practical devices for photocatalytic CO_2 conversion. For simplicity and to focus on evaluating materials, a closed batch reactor is the most commonly used system in the literature despite its limitations. However, for potential large-scale use in the future, rationally designed reactors such as a flow system would be beneficial, in which the light distribution and mass flow need to be considered carefully.[110] Only limited types of CO_2 conversion devices have been reported so far. Wang et al. reported a wireless and stand-alone photocatalyst sheet device for scalable solar formate production from carbon dioxide and water with the solar-to-formate efficiency of ∼0.1% using a nature-mimicking Z-scheme architecture.[43] Recently, a modular 5 kW pilot-scale solar-thermal system was demonstrated to synthesize methanol from H_2O and CO_2 captured directly from the ambient air operated under actual conditions.[111] This large-scale reactor could be an exciting reference for practical CO_2 conversion, although the device was only used in thermal catalysis so far. In the broad field of photocatalysis, a water-splitting device extended to the scale of 100 m^2 was preliminarily validated very recently, reaching a solar to hydrogen efficiency (STH) of 0.76%,[112] which to some extent demonstrated the safe, large-scale photocatalytic water splitting and gas collection and separation. However, the overall process was summed up as energy negative. A continuous flow reactor for scalable organosynthesis was also tested.[113] Another group of practical reactors for CO_2 photoreduction are the membrane reactors, which immobilize photocatalyst (nano)particles on the membrane substrates to replace a suspension.[114] Although such systems might suffer from possible catalyst losses under long-term operation, they have the advantages such as no need to separate the catalyst from the solution and highly stable catalytic efficiency.[115] The reported examples of such membrane reactors include C_3N_4 or TiO_2 on Nafion membrane,[116,117] TiO_2 on carbon paper,[118] TiO_2 and Cu−TiO_2 on zeolitic imidazolate framework (ZIF-8),[119] and so on, which are good examples for the potential use in a flow system. Reactors under concentrated solar power also have been developed to obtain the high density of electron−hole pairs in the photocatalyst, and the catalyst can also be heated to high temperatures.[73,120] We have also recently developed a flow-reactor for oxidative coupling of methane to C_2 products and a multilayer device for methanol reforming.[8,121] All these devices for the equivalent photocatalytic reactions might accelerate the development of efficient and scalable devices for practical CO_2 photoconversion, especially driven by the current global concern of the critical climate change.

Economic Considerations. The last challenge, closely connected to the third, is to take the cost of the reactant CO_2 into account, which is a limiting factor for scaling up but is often ignored. Most reports used CO_2 in significant excess without considering the cost of CO_2 capture processes or the conversion efficiency of CO_2. The approaches to directly capture CO_2 from the air include aqueous alkali capture (cost US \$97−134 tCO_2^{-1} for 0.1 MPa CO_2, US \$116−168 tCO_2^{-1} for 15.1 MPa CO_2), supported amine capture (cost ∼ US \$90 tCO_2^{-1}) and the disruptive solid absorption (cost ∼ US \$15−50 tCO_2^{-1}).[64,122,123] Besides, other criteria such as carbon intensity (CI, the amount of net carbon by weight emitted per unit of fuel energy consumed) and the full-cycle time should also be considered.[60] An analysis by Nitopi et al. showed that products such as methane and CO (syngas) are not economically feasible because their market prices do not make up for the energy cost of CO_2 capture, although these products are commonly reported in the literature.[16] Instead, more preferable C_1 products include methanol, formic acid, and CO (pure), while promising C_{2+} products are ethylene, ethanol, acetaldehyde, and propanol.[16] The direct reduction of CO_2 from the air is a very high cost and challenging process since CO_2 only accounts for ∼400 ppm in the atmosphere, and the existence of oxygen also tends to react with photoelectrons to form O_2^- competitively. A preliminary example is the photocatalytic CO_2 conversion directly from air with a ca. 98.35% selectivity to CH_3OH and ca. 4.32% conversion efficiency of CO_2 after 4 h reaction by selectively adsorbing CO_2 rather than O_2 on $Rb_{0.33}WO_3$ catalyst.[124] Clearly, this is promising, while the economic benefit is too early to assess. However, the development of routes for high value-added products could be promoted by the driving force from the market.

Overall, the photocatalytic efficiency of CO_2 to chemicals, in particular, the selectivity to the C_2 chemicals, remains moderate so far, and its economic and environmental feasibility should be evaluated carefully to avoid extra carbon emission. An in-depth understanding of the reaction pathway will enable

https://doi.org/10.1021/acscatal.2c01012
ACS Catal. 2022, 12, 7300−7316

a precise design of the photocatalytic system, including the semiconductor, surface modification, defect engineering, cocatalyst loading, reaction conditions, and so on, toward preferable products. All these are at a very early stage at present, requiring multidisciplinary efforts and collaborations to overcome the barriers facing.

AUTHOR INFORMATION

Corresponding Author

Junwang Tang − *Department of Chemical Engineering, University College London, London WC1E 7JE, U.K.;* orcid.org/0000-0002-2323-5510; Email: junwang.tang@ucl.ac.uk

Authors

Yiou Wang − *Department of Chemical Engineering, University College London, London WC1E 7JE, U.K.; Department of Physics, Ludwig-Maximilians-Universität München, 80539 Munich, Germany;* Present Address: Advanced Research Institute for Multidisciplinary Sciences, Beijing Institute of Technology, No. 5 South Zhongguancun Street, Beijing 100081, China

Enqi Chen − *Department of Chemical Engineering, University College London, London WC1E 7JE, U.K.*

Complete contact information is available at: https://pubs.acs.org/10.1021/acscatal.2c01012

Notes

The authors declare no competing financial interest.

ACKNOWLEDGMENTS

All authors are thankful for UK EPSRC (EP/S018204/2), Leverhulme Trust (RPG-2017-122), Royal Society Newton Advanced Fellowship grant (NAF\R1\191163), and Royal Society Leverhulme Trust Senior Research Fellowship (SRF \R1\21000153). Y.W. thanks the Alexander von Humboldt Foundation for a fellowship.

REFERENCES

(1) Etheridge, D. M.; Steele, L. P.; Langenfelds, R. L.; Francey, R. J.; Barnola, J.-M.; Morgan, V. I. Natural and anthropogenic changes in atmospheric CO2 over the last 1000 years from air in Antarctic ice and firn. *J. Geophys. Res.: Atmos.* **1996**, *101* (D2), 4115−4128.

(2) Smol, J. P. Climate Change: A planet in flux. *Nature* **2012**, *483* (7387), S12−S15.

(3) Oktyabrskiy, V. P. A new opinion of the greenhouse effect. *St. Petersburg Polytechnical University Journal: Physics and Mathematics* **2016**, *2* (2), 124−126.

(4) Sabine, C. L.; Heimann, M.; Artaxo, P.; Bakker, D. C.; Chen, C.-T. A.; Field, C. B.; Gruber, N.; Le Quéré, C.; Prinn, R. G.; Richey, J. E. Current status and past trends of the global carbon cycle. *The Global Carbon Cycle: Integrating Humans, Climate and the Natural World* **2004**, *62*, 17−44.

(5) Olah, G. A.; Prakash, G. K. S.; Goeppert, A. Anthropogenic Chemical Carbon Cycle for a Sustainable Future. *J. Am. Chem. Soc.* **2011**, *133* (33), 12881−12898.

(6) Murphy, J. L.; Measures, C. I. Ocean Acidification: The Role of CO_2. *Oceanography* **2014**, *27* (1), 238−246.

(7) Xie, H.; Yue, H.; Zhu, J.; Liang, B.; Li, C.; Wang, Y.; Xie, L.; Zhou, X. Scientific and Engineering Progress in CO2 mineralization Using Industrial Waste and Natural Minerals. *Engineering* **2015**, *1* (1), 150−157.

(8) Wang, Y.; Yao, E.-P.; Wu, L.; Feldmann, J.; Stolarczyk, J. K. A Multi-Layer Device for Light-Triggered Hydrogen Production from Alkaline Methanol. *Angew. Chem., Int. Ed.* **2021**, *60* (51), 26694.

(9) Randau, S.; Weber, D. A.; Kötz, O.; Koerver, R.; Braun, P.; Weber, A.; Ivers-Tiffée, E.; Adermann, T.; Kulisch, J.; Zeier, W. G.; Richter, F. H.; Janek, J. Benchmarking the performance of all-solid-state lithium batteries. *Nat. Energy* **2020**, *5* (3), 259−270.

(10) McKinlay, C. J.; Turnock, S. R.; Hudson, D. A. Route to zero emission shipping: Hydrogen, ammonia or methanol? *Int. J. Hydrogen Energy* **2021**, *46* (55), 28282−28297.

(11) Stolarczyk, J. K.; Bhattacharyya, S.; Polavarapu, L.; Feldmann, J. Challenges and Prospects in Solar Water Splitting and CO2 Reduction with Inorganic and Hybrid Nanostructures. *ACS Catal.* **2018**, *8* (4), 3602−3635.

(12) Hemminger, J. C.; Carr, R.; Somorjai, G. A. The photoassisted reaction of gaseous water and carbon dioxide adsorbed on the SrTiO3 (111) crystal face to form methane. *Chem. Phys. Lett.* **1978**, *57* (1), 100−104.

(13) Inoue, T.; Fujishima, A.; Konishi, S.; Honda, K. Photoelectrocatalytic reduction of carbon dioxide in aqueous suspensions of semiconductor powders. *Nature* **1979**, *277* (5698), 637−638.

(14) Walsh, J. J.; Jiang, C.; Tang, J.; Cowan, A. J. Photochemical CO_2 reduction using structurally controlled g-C3N4. *Phys. Chem. Chem. Phys.* **2016**, *18*, 24825−24829.

(15) Kong, D.; Han, X.; Xie, J.; Ruan, Q.; Windle, C. D.; Gadipelli, S.; Shen, K.; Bai, Z.; Guo, Z.; Tang, J. Tunable Covalent Triazine-based Frameworks (CTF-0) for Visible Light-Driven Hydrogen and Oxygen Generation from Water Splitting. *ACS Catal.* **2019**, *9*, 7697−7707.

(16) Nitopi, S.; Bertheussen, E.; Scott, S. B.; Liu, X.; Engstfeld, A. K.; Horch, S.; Seger, B.; Stephens, I. E. L.; Chan, K.; Hahn, C.; Nørskov, J. K.; Jaramillo, T. F.; Chorkendorff, I. Progress and Perspectives of Electrochemical CO2 Reduction on Copper in Aqueous Electrolyte. *Chem. Rev.* **2019**, *119* (12), 7610−7672.

(17) Albero, J.; Peng, Y.; García, H. Photocatalytic CO2 Reduction to C2+ Products. *ACS Catal.* **2020**, *10* (10), 5734−5749.

(18) Nordgren, J.; Selander, L.; Pettersson, L.; Nordling, C.; Siegbahn, K.; Ågren, H. Core state vibrational excitations and symmetry breaking in the CK and OK emission spectra of CO2. *J. Chem. Phys.* **1982**, *76* (8), 3928−3932.

(19) Freund, H. J.; Roberts, M. W. Surface chemistry of carbon dioxide. *Surf. Sci. Rep.* **1996**, *25* (8), 225−273.

(20) Indrakanti, V. P.; Kubicki, J. D.; Schobert, H. H. Photoinduced activation of CO2 on Ti-based heterogeneous catalysts: Current state, chemical physics-based insights and outlook. *Energy Environ. Sci.* **2009**, *2* (7), 745−758.

(21) Koppenol, W. H.; Rush, J. D. Reduction potential of the carbon dioxide/carbon dioxide radical anion: a comparison with other C1 radicals. *J. Phys. Chem.* **1987**, *91* (16), 4429−4430.

(22) Matsuoka, S.; Kohzuki, T.; Pac, C.; Ishida, A.; Takamuku, S.; Kusaba, M.; Nakashima, N.; Yanagida, S. Photocatalysis of oligo(p-phenylenes): photochemical reduction of carbon dioxide with triethylamine. *J. Phys. Chem.* **1992**, *96* (11), 4437−4442.

(23) Rasko, J.; Solymosi, F. Infrared Spectroscopic Study of the Photoinduced Activation of CO2 on TiO2 and Rh/TiO2 Catalysts. *J. Phys. Chem.* **1994**, *98* (29), 7147−7152.

(24) Indrakanti, V. P.; Schobert, H. H.; Kubicki, J. D. Quantum Mechanical Modeling of CO2 Interactions with Irradiated Stoichiometric and Oxygen-Deficient Anatase TiO2 Surfaces: Implications for the Photocatalytic Reduction of CO2. *Energy Fuels* **2009**, *23* (10), 5247−5256.

(25) Kamat, P. V. Manipulation of Charge Transfer Across Semiconductor Interface. A Criterion That Cannot Be Ignored in Photocatalyst Design. *J. Phys. Chem. Lett.* **2012**, *3* (5), 663−672.

(26) Yamazaki, Y.; Takeda, H.; Ishitani, O. Photocatalytic reduction of CO2 using metal complexes. *J. Photochem. Photobiol., C* **2015**, *25*, 106−137.

(27) Chang, X.; Wang, T.; Gong, J. CO2 photo-reduction: insights into CO2 activation and reaction on surfaces of photocatalysts. *Energy Environ. Sci.* **2016**, *9* (7), 2177−2196.

(28) Tang, J.; Durrant, J. R.; Klug, D. R. Mechanism of Photocatalytic Water Splitting in TiO2. Reaction of Water with

Photoholes, Importance of Charge Carrier Dynamics, and Evidence for Four-Hole Chemistry. *J. Am. Chem. Soc.* **2008**, *130* (42), 13885−13891.
(29) Fu, J.; Jiang, K.; Qiu, X.; Yu, J.; Liu, M. Product selectivity of photocatalytic CO2 reduction reactions. *Mater. Today* **2020**, *32*, 222−243.
(30) Henderson, M. A. A surface science perspective on TiO2 photocatalysis. *Surf. Sci. Rep.* **2011**, *66* (6), 185−297.
(31) Li, X.; Yu, J.; Jaroniec, M.; Chen, X. Cocatalysts for Selective Photoreduction of CO2 into Solar Fuels. *Chem. Rev.* **2019**, *119* (6), 3962−4179.
(32) Wang, Q.; Domen, K. Particulate Photocatalysts for Light-Driven Water Splitting: Mechanisms, Challenges, and Design Strategies. *Chem. Rev.* **2020**, *120* (2), 919−985.
(33) Kudo, A.; Miseki, Y. Heterogeneous photocatalyst materials for water splitting. *Chem. Soc. Rev.* **2009**, *38* (1), 253−278.
(34) Moniz, S. J. A.; Shevlin, S. A.; Martin, D. J.; Guo, Z.-X.; Tang, J. Visible-light driven heterojunction photocatalysts for water splitting − a critical review. *Energy Environ. Sci.* **2015**, *8* (3), 731−759.
(35) Hori, Y.; Wakebe, H.; Tsukamoto, T.; Koga, O. Electrocatalytic process of CO selectivity in electrochemical reduction of CO2 at metal electrodes in aqueous media. *Electrochim. Acta* **1994**, *39* (11), 1833−1839.
(36) Anpo, M.; Yamashita, H.; Ichihashi, Y.; Ehara, S. Photocatalytic reduction of CO2 with H2O on various titanium oxide catalysts. *J. Electroanal. Chem.* **1995**, *396* (1), 21−26.
(37) Tan, S. S.; Zou, L.; Hu, E. Kinetic modelling for photosynthesis of hydrogen and methane through catalytic reduction of carbon dioxide with water vapour. *Catal. Today* **2008**, *131* (1), 125−129.
(38) Peterson, A. A.; Abild-Pedersen, F.; Studt, F.; Rossmeisl, J.; Nørskov, J. K. How copper catalyzes the electroreduction of carbon dioxide into hydrocarbon fuels. *Energy Environ. Sci.* **2010**, *3* (9), 1311−1315.
(39) Hori, Y.; Murata, A.; Yoshinami, Y. Adsorption of CO, intermediately formed in electrochemical reduction of CO2, at a copper electrode. *J. Chem. Soc., Faraday Trans.* **1991**, *87* (1), 125−128.
(40) Shkrob, I. A.; Marin, T. W.; He, H.; Zapol, P. Photoredox Reactions and the Catalytic Cycle for Carbon Dioxide Fixation and Methanogenesis on Metal Oxides. *J. Phys. Chem. C* **2012**, *116* (17), 9450−9460.
(41) Wang, Y.; Liu, X.; Han, X.; Godin, R.; Chen, J.; Zhou, W.; Jiang, C.; Thompson, J. F.; Mustafa, K. B.; Shevlin, S. A.; Durrant, J. R.; Guo, Z.; Tang, J. Unique hole-accepting carbon-dots promoting selective carbon dioxide reduction nearly 100% to methanol by pure water. *Nat. Commun.* **2020**, *11* (1), 2531.
(42) Wang, Y.; Godin, R.; Durrant, J. R.; Tang, J. Efficient Hole Trapping in Carbon Dot/Oxygen-Modified Carbon Nitride Heterojunction Photocatalysts for Enhanced Methanol Production from CO2 under Neutral Conditions. *Angew. Chem., Int. Ed.* **2021**, *60* (38), 20811.
(43) Wang, Q.; Warnan, J.; Rodríguez-Jiménez, S.; Leung, J. J.; Kalathil, S.; Andrei, V.; Domen, K.; Reisner, E. Molecularly engineered photocatalyst sheet for scalable solar formate production from carbon dioxide and water. *Nat. Energy* **2020**, *5* (9), 703−710.
(44) Kortlever, R.; Shen, J.; Schouten, K. J. P.; Calle-Vallejo, F.; Koper, M. T. M. Catalysts and Reaction Pathways for the Electrochemical Reduction of Carbon Dioxide. *J. Phys. Chem. Lett.* **2015**, *6* (20), 4073−4082.
(45) Shkrob, I. A.; Dimitrijevic, N. M.; Marin, T. W.; He, H.; Zapol, P. Heteroatom-Transfer Coupled Photoreduction and Carbon Dioxide Fixation on Metal Oxides. *J. Phys. Chem. C* **2012**, *116* (17), 9461−9471.
(46) Sasirekha, N.; Basha, S. J. S.; Shanthi, K. Photocatalytic performance of Ru doped anatase mounted on silica for reduction of carbon dioxide. *Appl. Catal., B* **2006**, *62* (1), 169−180.
(47) Subrahmanyam, M.; Kaneco, S.; Alonso-Vante, N. A screening for the photo reduction of carbon dioxide supported on metal oxide catalysts for C1−C3 selectivity. *Appl. Catal., B* **1999**, *23* (2), 169−174.
(48) Koci, K.; Obalova, L.; Solcova, O. Kinetic study of photocatalytic reduction of CO2 over TiO2. *Chem. Process Eng.* **2010**, *31*, 395−407.
(49) Hori, Y.; Murata, A.; Takahashi, R. Formation of hydrocarbons in the electrochemical reduction of carbon dioxide at a copper electrode in aqueous solution. *J. Chem. Soc., Faraday Trans. 1* **1989**, *85* (8), 2309−2326.
(50) Cheng, T.; Xiao, H.; Goddard, W. A. Free-Energy Barriers and Reaction Mechanisms for the Electrochemical Reduction of CO on the Cu(100) Surface, Including Multiple Layers of Explicit Solvent at pH 0. *J. Phys. Chem. Lett.* **2015**, *6* (23), 4767−4773.
(51) Nie, X.; Esopi, M. R.; Janik, M. J.; Asthagiri, A. Selectivity of CO2 Reduction on Copper Electrodes: The Role of the Kinetics of Elementary Steps. *Angew. Chem., Int. Ed.* **2013**, *52* (9), 2459−2462.
(52) Park, H. R.; Pawar, A. U.; Pal, U.; Zhang, T.; Kang, Y. S. Enhanced solar photoreduction of CO2 to liquid fuel over rGO grafted NiO-CeO2 heterostructure nanocomposite. *Nano Energy* **2021**, *79*, 105483.
(53) DeWulf, D. W.; Jin, T.; Bard, A. J. Electrochemical and Surface Studies of Carbon Dioxide Reduction to Methane and Ethylene at Copper Electrodes in Aqueous Solutions. *J. Electrochem. Soc.* **1989**, *136* (6), 1686−1691.
(54) Liu, X.; Xiao, J.; Peng, H.; Hong, X.; Chan, K.; Nørskov, J. K. Understanding trends in electrochemical carbon dioxide reduction rates. *Nat. Commun.* **2017**, *8* (1), 15438.
(55) Schouten, K. J. P.; Kwon, Y.; van der Ham, C. J. M.; Qin, Z.; Koper, M. T. M. A new mechanism for the selectivity to C1 and C2 species in the electrochemical reduction of carbon dioxide on copper electrodes. *Chem. Sci.* **2011**, *2* (10), 1902−1909.
(56) Olah, G. A. Beyond Oil and Gas: The Methanol Economy. *Angew. Chem., Int. Ed.* **2005**, *44* (18), 2636−2639.
(57) Lin, L.; Zhou, W.; Gao, R.; Yao, S.; Zhang, X.; Xu, W.; Zheng, S.; Jiang, Z.; Yu, Q.; Li, Y.-W.; Shi, C.; Wen, X.-D.; Ma, D. Low-temperature hydrogen production from water and methanol using Pt/α-MoC catalysts. *Nature* **2017**, *544*, 80.
(58) Barreto, L.; Makihira, A.; Riahi, K. The hydrogen economy in the 21st century: a sustainable development scenario. *Int. J. Hydrogen Energy* **2003**, *28* (3), 267−284.
(59) Crabtree, G. W.; Dresselhaus, M. S.; Buchanan, M. V. The hydrogen economy. *Phys. Today* **2004**, *57* (12), 39−44.
(60) Tountas, A. A.; Ozin, G. A.; Sain, M. M. Solar methanol energy storage. *Nat. Catal.* **2021**, *4* (11), 934−942.
(61) Ikeue, K.; Yamashita, H.; Anpo, M.; Takewaki, T. Photocatalytic Reduction of CO2 with H2O on Ti−β Zeolite Photocatalysts: Effect of the Hydrophobic and Hydrophilic Properties. *J. Phys. Chem. B* **2001**, *105* (35), 8350−8355.
(62) Yamashita, H.; Fujii, Y.; Ichihashi, Y.; Zhang, S. G.; Ikeue, K.; Park, D. R.; Koyano, K.; Tatsumi, T.; Anpo, M. Selective formation of CH3OH in the photocatalytic reduction of CO2 with H2O on titanium oxides highly dispersed within zeolites and mesoporous molecular sieves. *Catal. Today* **1998**, *45* (1), 221−227.
(63) Lum, Y.; Cheng, T.; Goddard, W. A.; Ager, J. W. Electrochemical CO Reduction Builds Solvent Water into Oxygenate Products. *J. Am. Chem. Soc.* **2018**, *140* (30), 9337−9340.
(64) Fasihi, M.; Efimova, O.; Breyer, C. Techno-economic assessment of CO2 direct air capture plants. *J. Cleaner Prod.* **2019**, *224*, 957−980.
(65) Xie, J.; Jin, R.; Li, A.; Bi, Y.; Ruan, Q.; Deng, Y.; Zhang, Y.; Yao, S.; Sankar, G.; Ma, D.; Tang, J. Highly selective oxidation of methane to methanol at ambient conditions by titanium dioxide-supported iron species. *Nat. Catal.* **2018**, *1* (11), 889−896.
(66) Ji, Y.; Luo, Y. New Mechanism for Photocatalytic Reduction of CO2 on the Anatase TiO2(101) Surface: The Essential Role of Oxygen Vacancy. *J. Am. Chem. Soc.* **2016**, *138* (49), 15896−15902.
(67) Hao, Y.-C.; Chen, L.-W.; Li, J.; Guo, Y.; Su, X.; Shu, M.; Zhang, Q.; Gao, W.-Y.; Li, S.; Yu, Z.-L.; Gu, L.; Feng, X.; Yin, A.-X.; Si, R.; Zhang, Y.-W.; Wang, B.; Yan, C.-H. Metal-organic framework

https://doi.org/10.1021/acscatal.2c01012
ACS Catal. 2022, 12, 7300−7316

membranes with single-atomic centers for photocatalytic CO2 and O2 reduction. *Nat. Commun.* **2021**, *12* (1), 2682.
(68) Tahir, M. Synergistic effect in MMT-dispersed Au/TiO2 monolithic nanocatalyst for plasmon-absorption and metallic interband transitions dynamic CO2 photo-reduction to CO. *Appl. Catal., B* **2017**, *219*, 329−343.
(69) Gao, C.; Meng, Q.; Zhao, K.; Yin, H.; Wang, D.; Guo, J.; Zhao, S.; Chang, L.; He, M.; Li, Q.; Zhao, H.; Huang, X.; Gao, Y.; Tang, Z. Co3O4 Hexagonal Platelets with Controllable Facets Enabling Highly Efficient Visible-Light Photocatalytic Reduction of CO2. *Adv. Mater.* **2016**, *28* (30), 6485−6490.
(70) Kuriki, R.; Ishitani, O.; Maeda, K. Unique Solvent Effects on Visible-Light CO2 Reduction over Ruthenium(II)-Complex/Carbon Nitride Hybrid Photocatalysts. *ACS Appl. Mater. Interfaces* **2016**, *8* (9), 6011−6018.
(71) Xu, F.; Meng, K.; Cheng, B.; Wang, S.; Xu, J.; Yu, J. Unique S-scheme heterojunctions in self-assembled TiO2/CsPbBr3 hybrids for CO2 photoreduction. *Nat. Commun.* **2020**, *11* (1), 4613.
(72) Maeda, K.; Kuriki, R.; Zhang, M.; Wang, X.; Ishitani, O. The effect of the pore-wall structure of carbon nitride on photocatalytic CO2 reduction under visible light. *J. Mater. Chem. A* **2014**, *2* (36), 15146−15151.
(73) Guan, G.; Kida, T.; Harada, T.; Isayama, M.; Yoshida, A. Photoreduction of carbon dioxide with water over K2Ti6O13 photocatalyst combined with Cu/ZnO catalyst under concentrated sunlight. *Appl. Catal., A* **2003**, *249* (1), 11−18.
(74) Hou, W.; Hung, W. H.; Pavaskar, P.; Goeppert, A.; Aykol, M.; Cronin, S. B. Photocatalytic Conversion of CO2 to Hydrocarbon Fuels via Plasmon-Enhanced Absorption and Metallic Interband Transitions. *ACS Catal.* **2011**, *1* (8), 929−936.
(75) Duan, Y. Q.; Du, T.; Wang, X. W.; Cai, F. S.; Yuan, Z. H. Photoassisted CO_2 Conversion to Carbon by Reduced $NiFe_2O_4$. *Adv. Mater. Res.* **2013**, *726*−*731*, 420−424.
(76) Li, A.; Wang, T.; Li, C.; Huang, Z.; Luo, Z.; Gong, J. Adjusting the Reduction Potential of Electrons by Quantum Confinement for Selective Photoreduction of CO2 to Methanol. *Angew. Chem., Int. Ed.* **2019**, *58* (12), 3804−3808.
(77) Das, R.; Sarkar, S.; Kumar, R.; D. Ramarao, S.; Cherevotan, A.; Jasil, M.; Vinod, C. P.; Singh, A. K.; Peter, S. C. Noble-Metal-Free Heterojunction Photocatalyst for Selective CO2 Reduction to Methane upon Induced Strain Relaxation. *ACS Catal.* **2022**, *12* (1), 687−697.
(78) Albero, J.; Garcia, H.; Corma, A. Temperature Dependence of Solar Light Assisted CO2 Reduction on Ni Based Photocatalyst. *Top. Catal.* **2016**, *59* (8), 787−791.
(79) Wang, J.; Kim, E.; Kumar, D. P.; Rangappa, A. P.; Kim, Y.; Zhang, Y.; Kim, T. K. Highly Durable and Fully Dispersed Cobalt Diatomic Site Catalysts for CO2 Photoreduction to CH4. *Angew. Chem., Int. Ed.* **2022**, *61* (6), e202113044.
(80) Yu, S.; Wilson, A. J.; Heo, J.; Jain, P. K. Plasmonic Control of Multi-Electron Transfer and C−C Coupling in Visible-Light-Driven CO2 Reduction on Au Nanoparticles. *Nano Lett.* **2018**, *18* (4), 2189−2194.
(81) Luo, W.; Nie, X.; Janik, M. J.; Asthagiri, A. Facet Dependence of CO2 Reduction Paths on Cu Electrodes. *ACS Catal.* **2016**, *6* (1), 219−229.
(82) Park, H.; Ou, H.-H.; Colussi, A. J.; Hoffmann, M. R. Artificial Photosynthesis of C1−C3 Hydrocarbons from Water and CO2 on Titanate Nanotubes Decorated with Nanoparticle Elemental Copper and CdS Quantum Dots. *J. Phys. Chem. A* **2015**, *119* (19), 4658−4666.
(83) Sorcar, S.; Thompson, J.; Hwang, Y.; Park, Y. H.; Majima, T.; Grimes, C. A.; Durrant, J. R.; In, S.-I. High-rate solar-light photoconversion of CO2 to fuel: controllable transformation from C1 to C2 products. *Energy Environ. Sci.* **2018**, *11* (11), 3183−3193.
(84) Paul, J.; Hoffmann, F. M. Co2 conversion and oxalate stability on alkali promoted metal surfaces: Sodium modified Al(100). *Catal. Lett.* **1988**, *1* (12), 445−455.
(85) Schouten, K. J. P.; Pérez Gallent, E.; Koper, M. T. M. The influence of pH on the reduction of CO and CO2 to hydrocarbons on copper electrodes. *J. Electroanal. Chem.* **2014**, *716*, 53−57.
(86) Hori, Y.; Takahashi, I.; Koga, O.; Hoshi, N. Electrochemical reduction of carbon dioxide at various series of copper single crystal electrodes. *J. Mol. Catal. A: Chem.* **2003**, *199* (1), 39−47.
(87) Kuhl, K. P.; Cave, E. R.; Abram, D. N.; Jaramillo, T. F. New insights into the electrochemical reduction of carbon dioxide on metallic copper surfaces. *Energy Environ. Sci.* **2012**, *5* (5), 7050−7059.
(88) Liu, Q.; Cheng, H.; Chen, T.; Lo, T. W. B.; Xiang, Z.; Wang, F. Regulating the *OCCHO intermediate pathway towards highly selective photocatalytic CO2 reduction to CH3CHO over locally crystallized carbon nitride. *Energy Environ. Sci.* **2022**, *15* (1), 225−233.
(89) Zhu, S.; Li, X.; Jiao, X.; Shao, W.; Li, L.; Zu, X.; Hu, J.; Zhu, J.; Yan, W.; Wang, C.; Sun, Y.; Xie, Y. Selective CO2 Photoreduction into C2 Product Enabled by Charge-Polarized Metal Pair Sites. *Nano Lett.* **2021**, *21* (5), 2324−2331.
(90) Yu, F.; Jing, X.; Wang, Y.; Sun, M.; Duan, C. Hierarchically Porous Metal−Organic Framework/MoS2 Interface for Selective Photocatalytic Conversion of CO2 with H2O into CH3COOH. *Angew. Chem., Int. Ed.* **2021**, *60* (47), 24849−24853.
(91) Molino, A.; Mehariya, S.; Di Sanzo, G.; Larocca, V.; Martino, M.; Leone, G. P.; Marino, T.; Chianese, S.; Balducchi, R.; Musmarra, D. Recent developments in supercritical fluid extraction of bioactive compounds from microalgae: Role of key parameters, technological achievements and challenges. *J. CO2 Util.* **2020**, *36*, 196−209.
(92) Sun, S.; Watanabe, M.; Wu, J.; An, Q.; Ishihara, T. Ultrathin WO3·0.33H2O Nanotubes for CO2 Photoreduction to Acetate with High Selectivity. *J. Am. Chem. Soc.* **2018**, *140* (20), 6474−6482.
(93) Niu, P.; Yang, Y.; Yu, J. C.; Liu, G.; Cheng, H.-M. Switching the selectivity of the photoreduction reaction of carbon dioxide by controlling the band structure of a g-C3N4 photocatalyst. *Chem. Commun.* **2014**, *50* (74), 10837−10840.
(94) Shown, I.; Samireddi, S.; Chang, Y.-C.; Putikam, R.; Chang, P.-H.; Sabbah, A.; Fu, F.-Y.; Chen, W.-F.; Wu, C.-I.; Yu, T.-Y.; Chung, P.-W.; Lin, M. C.; Chen, L.-C.; Chen, K.-H. Carbon-doped SnS2 nanostructure as a high-efficiency solar fuel catalyst under visible light. *Nat. Commun.* **2018**, *9* (1), 169.
(95) Qian, X.; Yang, W.; Gao, S.; Xiao, J.; Basu, S.; Yoshimura, A.; Shi, Y.; Meunier, V.; Li, Q. Highly Selective, Defect-Induced Photocatalytic CO2 Reduction to Acetaldehyde by the Nb-Doped TiO2 Nanotube Array under Simulated Solar Illumination. *ACS Appl. Mater. Interfaces* **2020**, *12* (50), 55982−55993.
(96) Das, R.; Das, K.; Ray, B.; Vinod, C. P.; Peter, S. C. Green transformation of CO2 to ethanol using water and sunlight by the combined effect of naturally abundant red phosphorus and Bi2MoO6. *Energy Environ. Sci.* **2022**, *15*, 1967.
(97) Li, H.; Gan, S.; Wang, H.; Han, D.; Niu, L. Intercorrelated Superhybrid of AgBr Supported on Graphitic-C3N4-Decorated Nitrogen-Doped Graphene: High Engineering Photocatalytic Activities for Water Purification and CO2 Reduction. *Adv. Mater.* **2015**, *27* (43), 6906−6913.
(98) Dai, W.; Xu, H.; Yu, J.; Hu, X.; Luo, X.; Tu, X.; Yang, L. Photocatalytic reduction of CO2 into methanol and ethanol over conducting polymers modified Bi2WO6 microspheres under visible light. *Appl. Surf. Sci.* **2015**, *356*, 173−180.
(99) Dai, W.; Xiong, W.; Yu, J.; Zhang, S.; Li, B.; Yang, L.; Wang, T.; Luo, X.; Zou, J.; Luo, S. Bi2MoO6 Quantum Dots In Situ Grown on Reduced Graphene Oxide Layers: A Novel Electron-Rich Interface for Efficient CO2 Reduction. *ACS Appl. Mater. Interfaces* **2020**, *12* (23), 25861−25874.
(100) Yu, L.; Li, G.; Zhang, X.; Ba, X.; Shi, G.; Li, Y.; Wong, P. K.; Yu, J. C.; Yu, Y. Enhanced Activity and Stability of Carbon-Decorated Cuprous Oxide Mesoporous Nanorods for CO2 Reduction in Artificial Photosynthesis. *ACS Catal.* **2016**, *6* (10), 6444−6454.
(101) Adachi, K.; Ohta, K.; Mizuno, T. Photocatalytic reduction of carbon dioxide to hydrocarbon using copper-loaded titanium dioxide. *Sol. Energy* **1994**, *53* (2), 187−190.

https://doi.org/10.1021/acscatal.2c01012
ACS Catal. 2022, 12, 7300−7316

(102) Gui, M. M.; Wong, W. M. P.; Chai, S.-P.; Mohamed, A. R. One-pot synthesis of Ag-MWCNT@TiO2 core−shell nanocomposites for photocatalytic reduction of CO2 with water under visible light irradiation. *Chem. Eng. J.* **2015**, *278*, 272−278.
(103) Kim, W.; Seok, T.; Choi, W. Nafion layer-enhanced photosynthetic conversion of CO2 into hydrocarbons on TiO2 nanoparticles. *Energy Environ. Sci.* **2012**, *5* (3), 6066−6070.
(104) Chen, Q.; Chen, X.; Fang, M.; Chen, J.; Li, Y.; Xie, Z.; Kuang, Q.; Zheng, L. Photo-induced Au−Pd alloying at TiO2 {101} facets enables robust CO2 photocatalytic reduction into hydrocarbon fuels. *J. Mater. Chem. A* **2019**, *7* (3), 1334−1340.
(105) Garza, A. J.; Bell, A. T.; Head-Gordon, M. Mechanism of CO2 Reduction at Copper Surfaces: Pathways to C2 Products. *ACS Catal.* **2018**, *8* (2), 1490−1499.
(106) Sun, M.; Zhao, B.; Chen, F.; Liu, C.; Lu, S.; Yu, Y.; Zhang, B. Thermally-assisted photocatalytic CO2 reduction to fuels. *Chem. Eng. J.* **2021**, *408*, 127280.
(107) Kuehnel, M. F.; Orchard, K. L.; Dalle, K. E.; Reisner, E. Selective Photocatalytic CO2 Reduction in Water through Anchoring of a Molecular Ni Catalyst on CdS Nanocrystals. *J. Am. Chem. Soc.* **2017**, *139* (21), 7217−7223.
(108) Godin, R.; Wang, Y.; Zwijnenburg, M. A.; Tang, J.; Durrant, J. R. Time-Resolved Spectroscopic Investigation of Charge Trapping in Carbon Nitrides Photocatalysts for Hydrogen Generation. *J. Am. Chem. Soc.* **2017**, *139* (14), 5216−5224.
(109) Wang, Y.; Suzuki, H.; Xie, J.; Tomita, O.; Martin, D. J.; Higashi, M.; Kong, D.; Abe, R.; Tang, J. Mimicking Natural Photosynthesis: Solar to Renewable H2 Fuel Synthesis by Z-Scheme Water Splitting Systems. *Chem. Rev.* **2018**, *118* (10), 5201−5241.
(110) Guo, L.; Chen, Y.; Su, J.; Liu, M.; Liu, Y. Obstacles of solar-powered photocatalytic water splitting for hydrogen production: A perspective from energy flow and mass flow. *Energy* **2019**, *172*, 1079−1086.
(111) Schäppi, R.; Rutz, D.; Dähler, F.; Muroyama, A.; Haueter, P.; Lilliestam, J.; Patt, A.; Furler, P.; Steinfeld, A. Drop-in Fuels from Sunlight and Air. *Nature* **2022**, *601*, 63−68.
(112) Nishiyama, H.; Yamada, T.; Nakabayashi, M.; Maehara, Y.; Yamaguchi, M.; Kuromiya, Y.; Nagatsuma, Y.; Tokudome, H.; Akiyama, S.; Watanabe, T.; Narushima, R.; Okunaka, S.; Shibata, N.; Takata, T.; Hisatomi, T.; Domen, K. Photocatalytic solar hydrogen production from water on a 100-m2 scale. *Nature* **2021**, *598* (7880), 304−307.
(113) Yang, C.; Li, R.; Zhang, K. A. I.; Lin, W.; Landfester, K.; Wang, X. Heterogeneous photoredox flow chemistry for the scalable organosynthesis of fine chemicals. *Nat. Commun.* **2020**, *11* (1), 1239.
(114) Baniamer, M.; Aroujalian, A.; Sharifnia, S. Photocatalytic membrane reactor for simultaneous separation and photoreduction of CO2 to methanol. *Int. J. Energy Res.* **2021**, *45* (2), 2353−2366.
(115) Zhang, W.; Ding, L.; Luo, J.; Jaffrin, M. Y.; Tang, B. Membrane fouling in photocatalytic membrane reactors (PMRs) for water and wastewater treatment: A critical review. *Chem. Eng. J.* **2016**, *302*, 446−458.
(116) Pomilla, F. R.; Brunetti, A.; Marcì, G.; García-López, E. I.; Fontananova, E.; Palmisano, L.; Barbieri, G. CO2 to Liquid Fuels: Photocatalytic Conversion in a Continuous Membrane Reactor. *ACS Sustainable Chem. Eng.* **2018**, *6* (7), 8743−8753.
(117) Brunetti, A.; Pomilla, F. R.; Marcì, G.; Garcia-Lopez, E. I.; Fontananova, E.; Palmisano, L.; Barbieri, G. CO2 reduction by C3N4-TiO2 Nafion photocatalytic membrane reactor as a promising environmental pathway to solar fuels. *Appl. Catal., B* **2019**, *255*, 117779.
(118) Cheng, X.; Chen, R.; Zhu, X.; Liao, Q.; He, X.; Li, S.; Li, L. Optofluidic membrane microreactor for photocatalytic reduction of CO2. *Int. J. Hydrogen Energy* **2016**, *41* (4), 2457−2465.
(119) Maina, J. W.; Schütz, J. A.; Grundy, L.; Des Ligneris, E.; Yi, Z.; Kong, L.; Pozo-Gonzalo, C.; Ionescu, M.; Dumée, L. F. Inorganic Nanoparticles/Metal Organic Framework Hybrid Membrane Reactors for Efficient Photocatalytic Conversion of CO2. *ACS Appl. Mater. Interfaces* **2017**, *9* (40), 35010−35017.
(120) Guan, G.; Kida, T.; Yoshida, A. Reduction of carbon dioxide with water under concentrated sunlight using photocatalyst combined with Fe-based catalyst. *Appl. Catal., B* **2003**, *41* (4), 387−396.
(121) Li, X.; Xie, J.; Rao, H.; Wang, C.; Tang, J. Platinum- and CuOx-Decorated TiO2 Photocatalyst for Oxidative Coupling of Methane to C2 Hydrocarbons in a Flow Reactor. *Angew. Chem., Int. Ed.* **2020**, *59* (44), 19702−19707.
(122) Keith, D. W.; Holmes, G.; St. Angelo, D.; Heidel, K. A Process for Capturing CO2 from the Atmosphere. *Joule* **2018**, *2* (8), 1573−1594.
(123) Realmonte, G.; Drouet, L.; Gambhir, A.; Glynn, J.; Hawkes, A.; Köberle, A. C.; Tavoni, M. An inter-model assessment of the role of direct air capture in deep mitigation pathways. *Nat. Commun.* **2019**, *10* (1), 3277.
(124) Wu, X.; Li, Y.; Zhang, G.; Chen, H.; Li, J.; Wang, K.; Pan, Y.; Zhao, Y.; Sun, Y.; Xie, Y. Photocatalytic CO2 Conversion of M0.33WO3 Directly from the Air with High Selectivity: Insight into Full Spectrum-Induced Reaction Mechanism. *J. Am. Chem. Soc.* **2019**, *141* (13), 5267−5274.

https://doi.org/10.1021/acscatal.2c01012
ACS Catal. 2022, 12, 7300−7316